MODIFICATION OF THE EQUIVALENT CURRENT MODEL FOR A RECTANGULAR PLATE

J. R. Natzke
Radiation Laboratory
Department of Electrical Engineering
  and Computer Science
The University of Michigan
Ann Arbor, MI 48109

September, 1990

engy
UMR 0453

ABSTRACT

The equivalent current model of a perfectly conducting rectangular plate is modified to correct for singularities at and near grazing angles of incidence and observation and to account for the interaction between the corners of the plate. A traveling current wave model is applied to the edge currents of the plate, and empirical formulas are derived from data obtained using a CGFFT code. Results are obtained for the edge currents and for the far field backscatter for both principle polarizations.

TABLE OF CONTENTS

I. INTRODUCTION

Many techniques exist for determining the scattering from polygonal planar structures. Numerical techniques utilizing the method of moments, finite elements, and CGFFT methods provide rigorous solutions to the exact integral or differential equations characterizing the field behaviour of planar structures of any geometry. For structures having dimensions greater than several wavelengths, however, these numerical techniques become overly demanding as far as computation time and computer memory is concerned while ensuring adequate convergence of the solution. Thus high-frequency approximation techniques continue to be of great importance in the prediction of scattering from such structures.

The high-frequency techniques developed over the years such as geometric optics, physical optics, geometrical theory of diffraction, physical theory of diffraction, uniform theory of diffraction, and equivalent currents have limitations depending on the shape of the structure and direction of incidence, such as scattering directions and field singularities along shadow and reflection boundaries [1] [2]. With aspects of incidence and observation at or near normal for the perfectly conducting polygonal plates of interest here, physical optics gives a straight forward and accurate prediction of the scattering, since the surface current over the illuminated side of the plate gives the dominant scattering. Away from normal, though, the edges of the plate cause the dominant scattering effects. The equivalent current method then is of special interest in studying polygonal plates since the surface fields near the edges are collected at the edges and equated to fictitious edge currents [1]-[6], and the far scattered field is expressed as a contour integral of the currents

around the perimeter of the plate. This method also has the advantage over the other diffraction techniques in that the scattering can be predicted for arbitrary aspects of observation [3].

The equivalent current model has its limitations, especially in that it has current singularities at grazing directions of incidence and observation. The model also is lacking in that it does not predict the interaction of the surface currents between the edges and the coupling from one edge to another or the diffraction from the corners. One attempt at improving on this limitation was made in [7] by combining a first-order equivalent current model with a corner diffraction formulation, which was developed empirically. Results were presented for a variety of polygonal plates, but the direction of observation was limited to the plane of incidence. An approximation for the diffraction by the edge and vertex of a semi-infinite wedge was presented in [8]. The vertex diffraction is only presented for an edge wave excited by a dipole or plane wave at grazing angles. In [9], the geometrical theory of diffraction (GTD) was combined with the moment method to form a hybrid technique. The moment method subdomain basis functions were applied to regions on the plate where the GTD was inadequate, such as corners. In this way the hybrid model exactly accounts for the surface fields in the vicinity of regions which entire domain basis functions cannot characterize. The accuracy of this method greatly depends on the chosen combination of the basis functions, and the method is thus not completely rigorous without some prior knowledge of the scattering characteristics being investigated.

In this report we attempt to improve on the equivalent current model by investigating the actual currents along the edges of a perfectly conducting rectangular plate and then modeling them empirically. The process will certainly grant insight into the complex scattering mechanisms of the plate, such that applications of the model can be made to planar structures of other geometries and materials.

II. EDGE CURRENT ANALYSIS

A plane wave incident in the principal plane for a perfectly conducting rectangular plate is given by

$$\bar{H}^i(y,z) = - \hat{x} \, Y \, e^{-ik(y \sin\theta' - z \cos\theta')} \tag{1a}$$

$$\bar{E}^i(y,z) = \hat{x} \, e^{-ik(y \sin\theta' - z \cos\theta')} \tag{1b}$$

for H- and E-polarization, respectively, as shown in Fig. 1. This incident wave induces a surface current $\bar{J}$, which in turn can be considered the source of the field scattered from the plate. The scattered field is then characterized by the integral equation

$$\bar{E}^s(\bar{r}) = ikZ \iint_{S'} \bar{J}(\bar{r}') \cdot \left[\bar{\bar{I}} + \frac{1}{k^2} \nabla\nabla \right] G(\bar{r},\bar{r}') \, dS' \tag{2}$$

where $\bar{\bar{I}}$ is the unit dyad and $G(\bar{r},\bar{r}')$ is the free space Green's function. The surface integral is open since the plate is assumed to be infinitesimally thin. The surface current distribution in (2) can be determined by matching the scattered electric field to the incident electric field on S' such that the tangential component of the total electric field is zero over the plate surface. Once the surface current is calculated, the far field scattering is given by the radiation integral

$$\bar{E}^s(\bar{r}) = - ikZ \frac{e^{ikr}}{4\pi r} \iint_{S'} \hat{s} \times \hat{s} \times \bar{J}(\bar{r}') \, e^{-ik\hat{s} \cdot \bar{r}'} \, dS' \tag{3}$$

where $\hat{s}$ is the direction of scattering.

3

A. Equivalent Current Model

For far field scattering from plates of dimensions greater than several wavelengths, high frequency approximations can be made instead of solving (2) directly. The equivalent current (EC) model suggests that for high frequency plates, the diffracted field is attributed to fictitious equivalent currents flowing along the edges of the plate. That is, the surface currents near the edges are dominant scattering sources, especially away from normal angles of incidence. The diffracted field is then given by the contour integral

$$\bar{E}^d(\bar{r}) = -ik \frac{e^{ikr}}{4\pi r} \int_{C'} \left[Z\, I(\bar{r}')\, \hat{s} \times \hat{s} \times \hat{t} + M(\bar{r}')\, \hat{s} \times \hat{t} \right] e^{-ik\hat{s} \cdot \bar{r}'} \, dC' \tag{4}$$

where I and M are the electric and magnetic equivalent currents, respectively, and $\hat{t}$ is the vector direction of the edge contour C' which bounds S'. Expressions have been derived by Michaeli [3] for the edge currents in general by applying (3) to two perfectly conducting surfaces bounding a straight edge. Assuming the surface current is concentrated near the edge, an endpoint evalutation is performed for the integral in (3) which is normal to $\hat{t}$. In the high frequency limit for the length of the edge, the integral is solved for a canonical wedge problem or, for the problem at hand, a half plane. Matching this solution to the integrand of (4) gives expressions for I and M. Thus the equivalent currents I and M at the edge are effectively the average of the tangential and normal components, respectively, of the surface current $\bar{J}$ in the vicinity of the edge.

The first problem encountered in using Michaeli's solution is that the equivalent current coefficients become singular along the shadow and reflection boundaries. Michaeli presents a correction to the singularities in [4,5]. The singularities can also be resolved in a more straightforward manner by using the incremental length diffraction coefficients (ILDC) derived by Mitzner for the edge currents. Knott has shown that these ILDC can be seperated into Michaeli's current coefficients and a physical optics term, both of which are

4

singular on the shadow and reflection boundaries [4]. Since the ILDC contain the difference of these, the singularities of each cancel. The ILDC then account for the diffraction due only to the edges, and the scattering due to physical optics current integrated over the illuminated surface of the plate must also be added.

Other limitations of the model not corrected by Michaeli or the ILDC of Mitzner are apparent in the expressions for the equivalent currents. For the case of H-polarization (H-incident parallel to the leading edge of the plate) and backscatter, $\theta = \theta'$, Mitzner's EC model gives

$$M_1 = \frac{i}{k} \tan\theta' \left(\tan\frac{\theta'}{2} - 1 \right) e^{-i\frac{kL}{2}\cos\theta'} \tag{5a}$$

$$I_2 = \frac{i}{kZ} \frac{1}{\sin\theta'} e^{ikz\cos\theta'} \tag{5b}$$

$$M_3 = -\frac{i}{k} \tan\theta' \left(\cot\frac{\theta'}{2} - 1 \right) e^{i\frac{kL}{2}\cos\theta'} \tag{5c}$$

$$I_4 = \frac{i}{kZ} \frac{1}{\sin\theta'} e^{ikz\cos\theta'} \tag{5d}$$

where the subscripts denote the edges as labeled in Fig. 1. At grazing, $\theta' = 0$, the current on the plate should become zero for this polarization. The front edge current M_1 becomes zero as expected. However, (5b) and (5d) show that the side edge currents I_2 and I_4 become singular, and from (5c), the back edge current M_3 approaches a finite, nonzero value. When the incident field is E-polarized (E-incident parallel to the leading edge of the plate), the equivalent currents on each edge are

$$I_1 = \frac{i}{kZ} (1 - \tan\theta' + \sec\theta') e^{-i\frac{kL}{2}\cos\theta'} \tag{6a}$$

5

$$I_2 = -\frac{i2}{kZ}\cot\theta' \, e^{ikz\cos\theta'} \tag{6b}$$

$$M_2 = \frac{i}{k}\frac{1}{\sin\theta'} e^{ikz\cos\theta'} \tag{6c}$$

$$I_3 = \frac{i}{kZ}(1 + \tan\theta' - \sec\theta')e^{i\frac{kL}{2}\cos\theta'} \tag{6d}$$

$$I_4 = \frac{i2}{kZ}\cot\theta' \, e^{ikz\cos\theta'} \tag{6e}$$

$$M_4 = \frac{i}{k}\frac{1}{\sin\theta'} e^{ikz\cos\theta'} \tag{6f}$$

and it is noted that the side edges have both electric and magnetic equivalent currents. At grazing angles of incidence, the plate has a finite surface current for this case. The front edge current I_1 becomes a maximum and is finite at grazing as expected, while the side edge currents become singular and the back edge current approaches zero.

It is also apparent that the EC model does not account for the interaction between the corners of the plate , since infinite edges were assumed for the canonical solutions. Any coupling from one edge current to another via the corners or the plate surface has also not been included since each edge current coefficient is calculated independently of the location of the others. And the cross coupling between the two vector components of the surface current caused by the finite dimensions of the plate would produce both electric and magnetic equivalent currents for each edge, but such is not the case for the EC model. The task at hand then is to determine which of these factors might be used to improve the EC model by removing the singularities of the side edges and correcting the back edge currents. The investigation may also reveal other dominant scattering mechanisms not accounted for in the EC model.

6

B. Side Edge Currents

To analyze the actual side edge currents, the surface currents were generated using a CGFFT program, which gives a numerical solution to (2). The program was run for a 2λ by 4λ rectangular plate, with sampling elements of $1/20\lambda$ by $1/20\lambda$ and a 3.5 percent tolerance of convergence. The tangential surface current component along edge 2 and $1/40\lambda$ from the edge is plotted in Figs. 2 to 5 for H- and E-polarizations. The two angles of incidence considered are $\theta' = 10, 60$ degrees. The oscillations observed in the current distribution near grazing angles indicate a strong interaction between the front and back corners of the side edge. Using a traveling current wave viewpoint, the current induced by the incident field on the edge of the plate experiences a reflection and transmission at each of the corners. The reflected waves are guided by the edge as they travel back and forth, continually reflected at the corners with transmission (corner coupling and radiation) occuring as well. The net traveling current on the edge could then be represented by the superposition of three components, the *forced* component flowing with the incident field and two *reflected* components traveling in opposite directions from each corner. The forced component travels with the phase velocity of the incident field along the edge, and we will assume that the reflected components have the propagation constant of free space. A general expression for the electric current along the side edge is then

$$I_2 = a(\theta') \, e^{ikz \, \cos\theta'} + b(\theta') \, e^{ikz} + c(\theta') \, e^{-ikz} \tag{7}$$

efficients a, b, and c are assumed to be independent of z.

Given that the three components of (7) are traveling with three different velocities, they also have three different spatial frequencies. The Fourier transform of (7) with respect to z is

7

$$\tilde{I}_2 = 2\pi L \left[a(\theta') \; \text{sinc}\frac{L}{2}(k_z\text{-}k \; \text{cos}\theta') + b(\theta') \; \text{sinc}\frac{L}{2}(k_z\text{-}k) + c(\theta') \; \text{sinc}\frac{L}{2}(k_z\text{+}k) \right] \qquad (8)$$

where k_z denotes the spectral domain. To verify this traveling wave viewpoint, the edge current data of Figs. 2 to 5 was Fourier transformed numerically, with the results plotted in Figs. 6 to 9. To make a comparison, the coefficients a, b, and c were calculated by point matching (7) to the plate data at the zeros of the arguments of the sinc functions. For H-polarization,

$$a(10°) = 17.2e^{-i1.6}, \quad b(10°) = 17.1e^{i1.61}, \quad c(10°) = 1.9e^{i0.7}$$

$$a(60°) = 4.4e^{-i2.4}, \quad b(60°) = 2.1e^{i2.35}, \quad c(60°) = 2.4e^{-i0.78}$$

and (7) was plotted in Figs. 6 and 7 using these values. As shown, excellent results are obtained for both angles of incidence. For E-polarization, the point-matching yielded

$$a(10°) = 9.6e^{i2.56}, \quad b(10°) = 13.0e^{i0.02}, \quad c(10°) = 1.4e^{-i0.78}$$

$$a(60°) = 1.6e^{i1.15}, \quad b(60°) = 0.2e^{i0.02}, \quad c(60°) = 0.15e^{i0.78}.$$

Again, excellent results were obtained for $\theta' = 10$ degrees as plotted in Fig. 8, but for $\theta' = 60$ degrees, it is seen in Fig. 9 that the peaks do not coincide exactly for the a component.

The approximation to the edge current was compared to the plate data by plotting (7) in Figs. 2 to 5 using the above component coefficients. In Fig. 2, the approximation to the current is in good agreement with the plate data. The current of (7) does not show the same increasing amplitude of the oscillation with z since any "standing" (non-propagating) currents near the corners were not accounted for. The accuracy of assuming k as the propagation constant of the b, and c components has also not been verified. The same is the case for the comparison in Figs. 3 and 4. In Fig. 5, E-polarization with $\theta' = 60$ degrees, the component curve gives a good average value of the edge current but does not

characterize its shape as in the previous cases. This points again to the discrepency noted in the Fourier transform plot of Fig. 9. In spite of the differences in the current plots, the comparisons of the Fourier transforms of the current gives evidence that the *dominant* current components have been identified.

C. Back Edge Currents

As mentioned above, the back edge currents need to be corrected or modified for both polarizations. For *H*-polarization, the back edge current is a magnetic one, which can not be obtained from the electric surface current data of the plate directly. This magnetic current is associated with the surface current normal to the back edge and is an isolated effect in the EC model. What actually occurs is a strong coupling between the front and back edges over the surface of the plate near grazing angles of incidence due to the surface current normal to these edges. Thus for plates of high frequency widths W we will use the solution to an infinite strip with a cross section of L to represent the scattering from the edges 1 and 3 and from the surface [10]. This solution accounts for the edge currents M_1 and M_3 of (5) and the PO surface current and will be presented in a later section.

For *E*-polarization, there is very little coupling between the front and back edges of the plate, and thus the strip model would not provide any improvement to the back edge current near and at grazing. Given the strong front edge current at grazing angles of incidence, though, a coupling would occur around the corners and along the sides to the back edge, providing a finite current. This has been verified experimentally by Knott, Liepa, and Senior [10] by placing notches on the side edges and observing their effect on backscatter. As previously mentioned, this coupling is completely unaccounted for by the EC model. Using a similar three component current model as for the side edge currents, the back edge electric current is represented by

$$I_3 = a(\theta') + b(\theta') \, e^{ikx} + c(\theta') \, e^{-ikx} \qquad (9)$$

9

with the complex coefficients assumed to be independent of x. The validity of this model is verified in Fig. 10, in which the back edge current from the CGFFT code is plotted along with (9) for $\theta' = 10$ degrees. The coefficients of (9) were determined by point matching in the spectral domain, giving

$$a(10°) = 1.1e^{-i2.96} , \quad b(10°) = 1.5e^{i0.78} , \quad c(10°) = 1.5e^{i0.78} .$$

III. MODIFIED EQUIVALENT CURRENTS

A. Side Edge Currents

Of first concern is the modeling of the side edge currents for both polarizations. For the traveling wave viewpoint applied to the side edge currents, the components b and c are described as the reflections of the component a. This would imply a type of transmission line model of the edge current, with reflection and transmission coefficients characterizing the corners. The reflection coefficients would give the coupling between b and c and the component a at their respective corners, while the transmission coefficients would describe the coupling of a to the adjacent edges. The other coupling which occurs with the two components of the surface current on the plate will be assumed negligible in this development. To observe the nature of the incident aspect dependence of the coefficients, a, b, and c were calculated by point matching (8) to the spatial Fourier transform of the CGFFT current data along edge 2. The results for a, b, and c are plotted in Figs. 11 to 13 for H-polarization and in Figs. 14 to 16 for E-polarization.

For H-polarization, it is apparent from Fig. 11 that the coefficient a correlates directly with the electric EC model expressions for the side edges, having the same singular behaviour. That is,

10

$$a(\theta') = i\,\frac{a_o}{\sin\theta'} \qquad\qquad (10)$$

where $a_o = -3.423$, the normalizing factor for $a(\pi/2)$, to match (10) to the data, as plotted in Fig. 11. To match with the EC expression in (5b) or (5d), $a_o = 1/kZ$. For the coefficient b,

$$b(\theta') = a(\theta')\,\Gamma_{ba}\;, \qquad\qquad (11a)$$

and from curve fitting to the plot of Fig. 12, an approximation to the reflection coefficient at $z = -L/2$ is

$$\Gamma_{ba} = -\cos(0.8\theta')\,e^{-i\frac{kL}{2}(\cos\theta' - 1)} \qquad\qquad (11b)$$

where the phase term is due to the location of the phase center at $z = 0$. The magnitude of b relative to a is independent of L. The singularity of a at grazing then is cancelled by its reflection at $z = -L/2$, the b component, since the reflection coefficient approaches -1 as θ' approaches zero. The expression (11) is plotted in Fig. 12 for comparison. For the coefficient c,

$$c(\theta') = a(\theta')\,\Gamma_{ca} + b(\theta')\,\Gamma_{cb}$$
$$= a(\theta')\left[\Gamma_{ca} + \Gamma_{ba}\,\Gamma_{cb}\right] \qquad\qquad (12a)$$

where the component c must be given by the reflection of b in addition to a such that the singularity of a is cancelled at grazing. For the reflection coefficients, it is known that (a) $|\Gamma_{ca}| \cong 0.3$ at normal incidence according to Figs. 11 and 13, (b) that Γ_{ca} approaches Γ_{cb} near grazing, since the phase velocity of the a component approaches that of the b component, and (c) Γ_{cb} is constant with angle of incidence. Also, Γ_{ca} could very well have an angle dependence. As a first approximation, though, let $|\Gamma_{ca}| = |\Gamma_{cb}|$ such that

$$\Gamma_{ca} = -0.3 \, e^{i\frac{kL}{2}(\cos\theta' + 1)} \tag{12b}$$

$$\Gamma_{cb} = -0.3 \, e^{ikL} \,, \tag{12c}$$

and the results are shown in Fig. 13. The interaction of a and b at $z = L/2$ is seen by the oscillating curve. At grazing, $|c|$ goes to zero as the reflections of a and b from $z = L/2$ cancel each other. Using the coefficients of (10) in (7) gives the modified equivalent currents for I_2 in (5b), and it was verified that identical results are obtained for I_4 in (5d).

For E-polarization, from Fig. 14, the empirical results gave

$$a(\theta') = -i \, a_o \cot\theta' \tag{13}$$

where $a_o = -2.512$ to give the best fit of (13) to the actual data for $a(\theta')$. For the electric side edge currents of the EC model, $a_o = 2/kZ$ in (6a) and (6e). For the reflected component b, a comparison of Figs. 14 and 15 reveals that $|b| > |a|$ near grazing. This is due to the contribution to b by the coupling around the corner of the forced component a on the front edge of the plate. Considering the side edge currents alone, the sum of a and b must give a nonzero, finite current at grazing. The summation of the data for a and b results in a curve of constant slope with angle, with a magnitude of ~ 0.5 at normal and ~ 6.0 near grazing. Apparently then b successfully cancels the infinity of a and provides a constant current at grazing. To accomplish this, it is proposed that

$$b(\theta') = a(\theta') \, \Gamma_{ba} \,, \tag{14a}$$

where

$$\Gamma_{ba} = -(\sec\theta' - \tan\theta') \, e^{-i\frac{kL}{2}(\cos\theta' - 1)} \,. \tag{14b}$$

12

Apart from the phase term, the reflection coefficient is again negative. The plot of (14) is included in Fig. 15, where an exact correlation is not expected because of the coupling from the front and back edges. Following the same notion for the c component of the H-polarization case, the coefficient c for E-polarization is

$$c(\theta') = a(\theta') \left[\Gamma_{ca} + \Gamma_{ba} \Gamma_{cb} \right] , \qquad (15)$$

and the reflection coefficients are those from (12b) and (12c). These coefficients give the modified equivalent currents for I_2 and I_4 in (6b) and (6e).

The modified equivalent current (MEC) model was compared to the edge current data from the CGFFT code by using the coefficients of (10) through (15) in (7). For H-polarization, the results are shown in Figs. 17 and 18. The results are in good comparison near grazing, but deviate from the CGFFT data at $\theta' = 60$ degrees in Fig. 18 since the empirical formulas for b and c in (11a) and (12a) only account for first order reflections and because of the approximation $|\Gamma_{ca}| = |\Gamma_{cb}|$. The E-polarization results are shown in Figs. 19 and 20. In Fig. 19 the CGFFT curve has almost twice the amplitude of the MEC curve since there is a strong contribution from the front edge not accounted for in (11). The amplitudes are more closely matched in Fig. 20 for $\theta' = 60$ degrees. Thus the reflected current components added to the EC model for the side edge electric currents have removed the singularity and have given a good characterization of the interaction between the corners.

B. Back Edge Currents

Using the proposed current expression in (9) for the back edge, the coefficients were calculated as a function of angle of incidence. Figure 21 shows the results for a, and this coefficient does not become zero at grazing as the EC model gives a zero for I_3 in (6d). A correction then to I_3 to fit an empirical expression to the data yields

13

$$a(\theta') = i\, a_o \left[1 + 0.7\, (\tan\theta' - \sec\theta') \right] e^{i\frac{kL}{2}\cos\theta'} \tag{16}$$

where $a_o = -3.0$. For the electric back edge current of the EC model, $a_o = 1/kZ$ in (6a). The data for b is plotted in Fig. 22. The reflection coefficient at $x = -W/2$ is expected to the the same as the reflection coefficients for the side edge for H-polarization at normal incidence. So with b given again by (11a), the reflection of a for the back edge is now

$$\Gamma_{ba} = -0.3\, e^{i\frac{kW}{2}} . \tag{17}$$

The empirical result in the magnitude plot of Fig. 22 shows a discrepency in the accuracy of (17) because the coupling from the side edges was not accounted for, which would increase the magnitude significantly. The data showed that for the c component,

$$c(\theta') = b(\theta') \tag{18}$$

for all angles of incidence. This is expected since the reflection of the component a is the same at each corner. Figure 23 shows the results for the coefficients of (16) to (18) used in (9), as compared to the CGFFT data. The discrepancy is again due to the exclusion of the corner coupling effects, which have yet to be modeled.

IV. FAR FIELD SCATTERING

The far field scattering from the rectangular plate is expressed as a combination of (3) and (4) for the modeled surface and edge currents, respectively. For H-polarization, the backscattered field is

$$E_\theta^s(r,\theta) = \frac{e^{-ikr}}{r}\left[S_2(\theta) + S_4(\theta) + S_{st}(\theta)\right]$$ (19)

where the far field amplitudes are

$$S_2 = \frac{ikZ}{4\pi}L\,\sin\theta\left[a_2(\theta')\,\operatorname{sinc}\frac{kL}{2}(\cos\theta + \cos\theta') + b_2(\theta')\,\operatorname{sinc}\frac{kL}{2}(\cos\theta + 1)\right.$$
$$\left. + c_2(\theta')\,\operatorname{sinc}\frac{kL}{2}(\cos\theta - 1)\right]$$ (20)

$$S_4 = \frac{ikZ}{4\pi}L\,\sin\theta\left[a_4(\theta')\,\operatorname{sinc}\frac{kL}{2}(\cos\theta + \cos\theta') + b_4(\theta')\,\operatorname{sinc}\frac{kL}{2}(\cos\theta + 1)\right.$$
$$\left. + c_4(\theta')\,\operatorname{sinc}\frac{kL}{2}(\cos\theta - 1)\right]$$ (21)

from (10) to (12) in (4) and

$$S_{st} = \frac{i}{4}\sqrt{\frac{2}{k\pi}}\left\{\frac{1-\cos\theta}{\cos\theta}e^{-ikL\cos\theta}\left[1 - \frac{2}{\sqrt{\pi}}e^{-i\frac{\pi}{4}}\sin\frac{\theta}{2}\,F\left(\sqrt{2kL}\,\cos\frac{\theta}{2}\right)\right]^2\right.$$
$$\left. - \frac{1+\cos\theta}{\cos\theta}e^{ikL\cos\theta}\left[1 - \frac{2}{\sqrt{\pi}}e^{-i\frac{\pi}{4}}\cos\frac{\theta}{2}\,F\left(\sqrt{2kL}\,\sin\frac{\theta}{2}\right)\right]^2\right\}$$ (22)

from [10], where $F(\tau)$ is the Fresnel integral

$$F(\tau) = \int_\tau^\infty e^{iu^2}\,du\ .$$

The far field amplitude for the strip is only presented for the backscatter case. The backscatter cross section of a 2λ by 4λ rectangular plate was calculated using the CGFFFT code and (19), and the comparison is shown in Fig. 24. The main contribution to the total scattering is from the term S_{st}, with S_2 and S_4 adding to the peak of the traveling wave

lobe. The results are in good agreement except for the null of the traveling wave lobe near grazing.

For E-polarization, the scattered far field is given by

$$E_x^s(r,\theta) = \frac{e^{ikr}}{r} \left[S_1(\theta) + S_3(\theta) + S_{PO}(\theta) \right] \tag{23}$$

where the far field amplitudes are

$$S_1 = \frac{ikZ}{4\pi} W \left[\frac{i}{kZ} (1 - \tan\theta' + \sec\theta') \, e^{-i\frac{kL}{2}\cos\theta'} \right] e^{-i\frac{kL}{2}\cos\theta} \tag{24}$$

from (6a) in (4),

$$S_3 = \frac{ikZ}{4\pi} W \left[a_3(\theta') + b_3(\theta') \, \mathrm{sinc}\frac{kW}{2} + c_3(\theta') \, \mathrm{sinc}\frac{kW}{2} \right] e^{i\frac{kL}{2}\cos\theta} \tag{25}$$

from (13) to (15) in (4), and

$$S_{PO} = \frac{ik}{2\pi} WL \sin\theta' \, \mathrm{sinc}\frac{kL}{2}(\cos\theta + \cos\theta') \tag{26}$$

from the PO surface current in (3). Because of the phase difference between the electric currents on the side edges, their contributions to the scattering in the principal plane cancel each other. The plot of (23) is compared to CGFFT results for backscatter from the rectangular plate, as the plot of the cross section in Fig. 25 shows. For the choice of $W = 2\lambda$, the b and c coefficients of the back edge do not contribute to the scattered field. The discrepancy in the comparison of the MEC to the CGFFT results is then only due to the a coefficients of the front and back edges and the PO term.

16

V. CONCLUSIONS

The physical interpretation of the side edge currents as traveling wave currents has proven to be valid and to be at least empirically quantifiable. The MEC model has removed the singularities of the current for aspects at grazing. Considering higher order interactions would undoubtedly improve the MEC results, as well as investigating the actual propagation constants of the b and c components. The model must also be validated for plates of other dimensions.

REFERENCES

[1]   E. F. Knott, "A Progression of High-Frequency RCS Prediction Techniques," *Proc. IEEE*, vol. 73, no. 2, pp. 252-264, Feb. 1985.

[2]   E. F. Knott and T. B. A. Senior, "Comparison of Three High-Frequency Diffraction Techniques," *Proc. IEEE*, vol. 62, no. 11, pp. 1468-1474, Nov. 1974.

[3]   A. Michaeli, "Equivalent Edge Currents for Arbitrary Aspects of Observation," *IEEE Trans. Antennas Propagat.*, vol. AP-32, no. 3, pp. 252-258, Mar. 1984.

[4]   A. Michaeli, "Elimination of Infinities in Equivalent Edge Currents, Part I: Fringe Current Components," *IEEE Trans. Antennas Propagat.*, vol. AP-34, no. 7, pp. 912-918, July 1986.

[5]   A. Michaeli, "Elimination of Infinities in Equivalent Edge Currents, Part II: Physical Optics Components," *IEEE Trans. Antennas Propagat.*, vol. AP-34, no. 8, pp. 1034-1037, Aug. 1986.

[6]   E. F. Knott, "The Relationship Between Mitzner's ILDC and Michaeli's Equivalent Currents," *IEEE Trans. Antennas Propagat.*, vol. AP-33, no. 1, pp. 112-114, Jan. 1985.

[7]   F. A. Sikta, W. D. Burnside, T-T. Chu, and L. Peters, Jr., "First-Order Equivalent Current and Corner Diffraction Scattering from Flat Plate Structures," *IEEE Trans. Antennas Propagat.*, vol. AP-31, no. 4, pp. 584-584, July 1983.

[8]   L. P. Ivrissimtzis and R. J. Marhefka, "Edge Wave Vertex and Edge Diffraction," *Radio Science*, vol. 24, no. 6, pp. 771-784, Nov.-Dec. 1989.

[9]   A. H. Chang and R. Mittra, "Using Half-Plane Solutions in the Context of MM for Analyzing Large Flat Structures with or without Resistive Loadings," *IEEE Trans. Antennas Propagat.*, vol. AP-38, no. 7, pp. 1001-1009, July 1990.

[10] E. F. Knott, V. V. Liepa, and T. B. A. Senior, "Plates and Edges," *IEEE Trans. Antennas Propagat.*, vol. AP-19, no. 11, pp. 788-789, Nov. 1971.

[11] T. B. A. Senior and S. I. Yang, "Travelling Waves on Thin Bodies," *Electronic Letters*, pp. 1050-1051, 6 Dec. 1984.
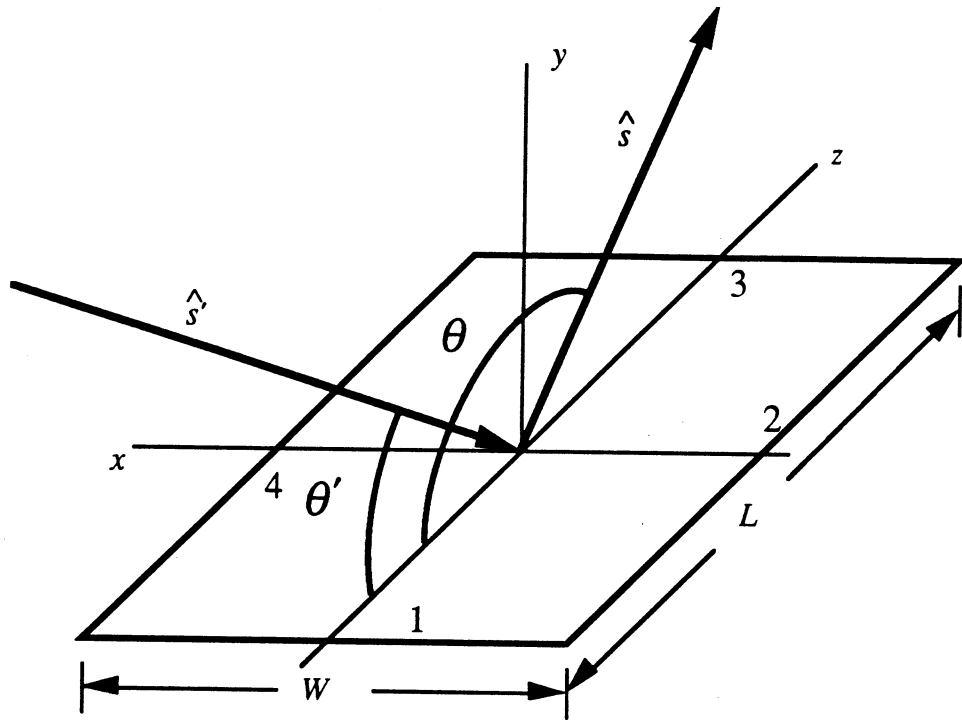
Figure 1. Rectangular plate configuration
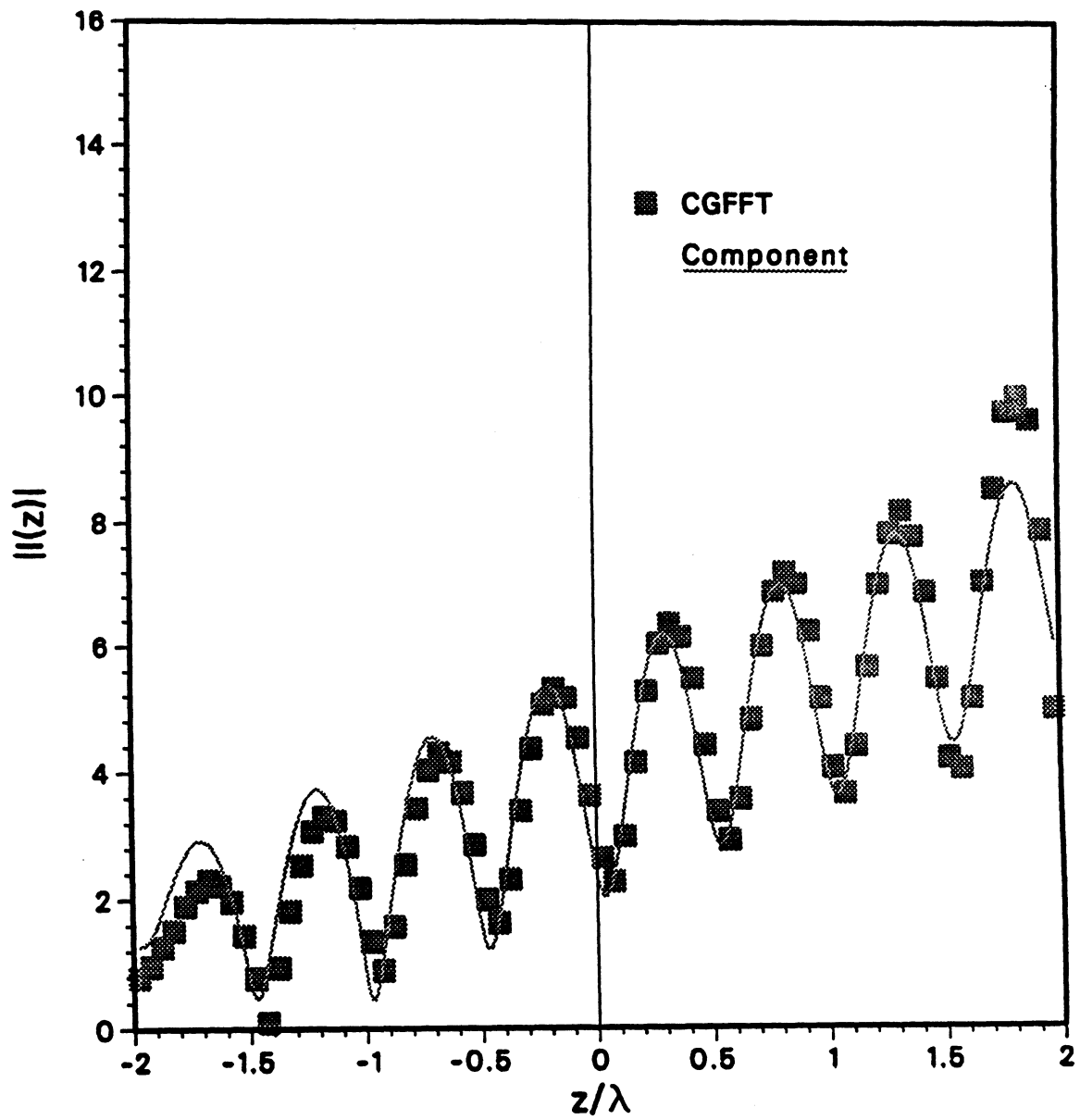
Figure 2.   H-polarization, side edge current on edge 2
of the plate, $\theta' = 10°$, W=2λ, L =4λ.
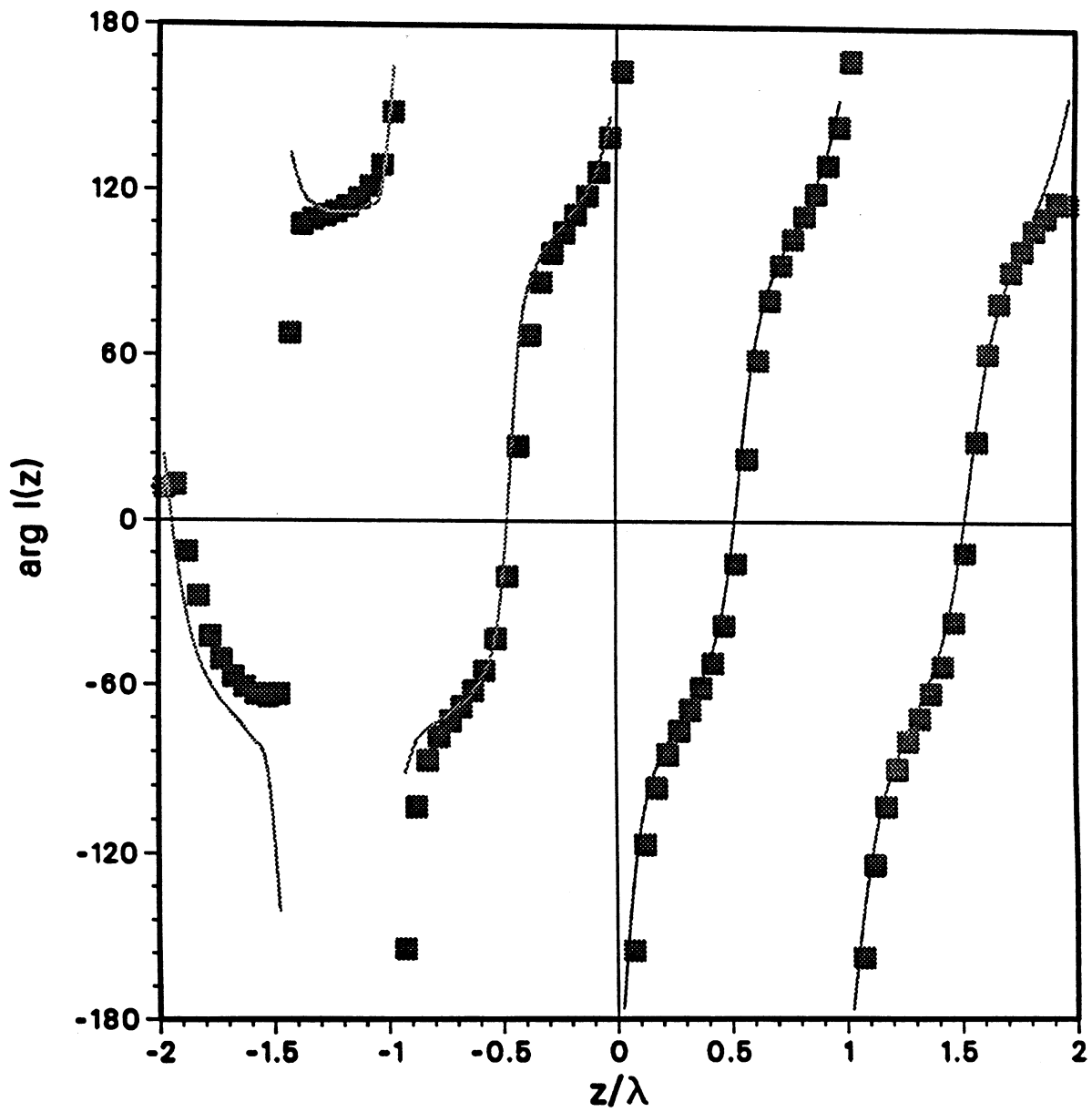
Figure 2b.   H-polarization, side edge current on edge 2
of the plate, $\theta' = 10°$, W=2λ, L=4λ.
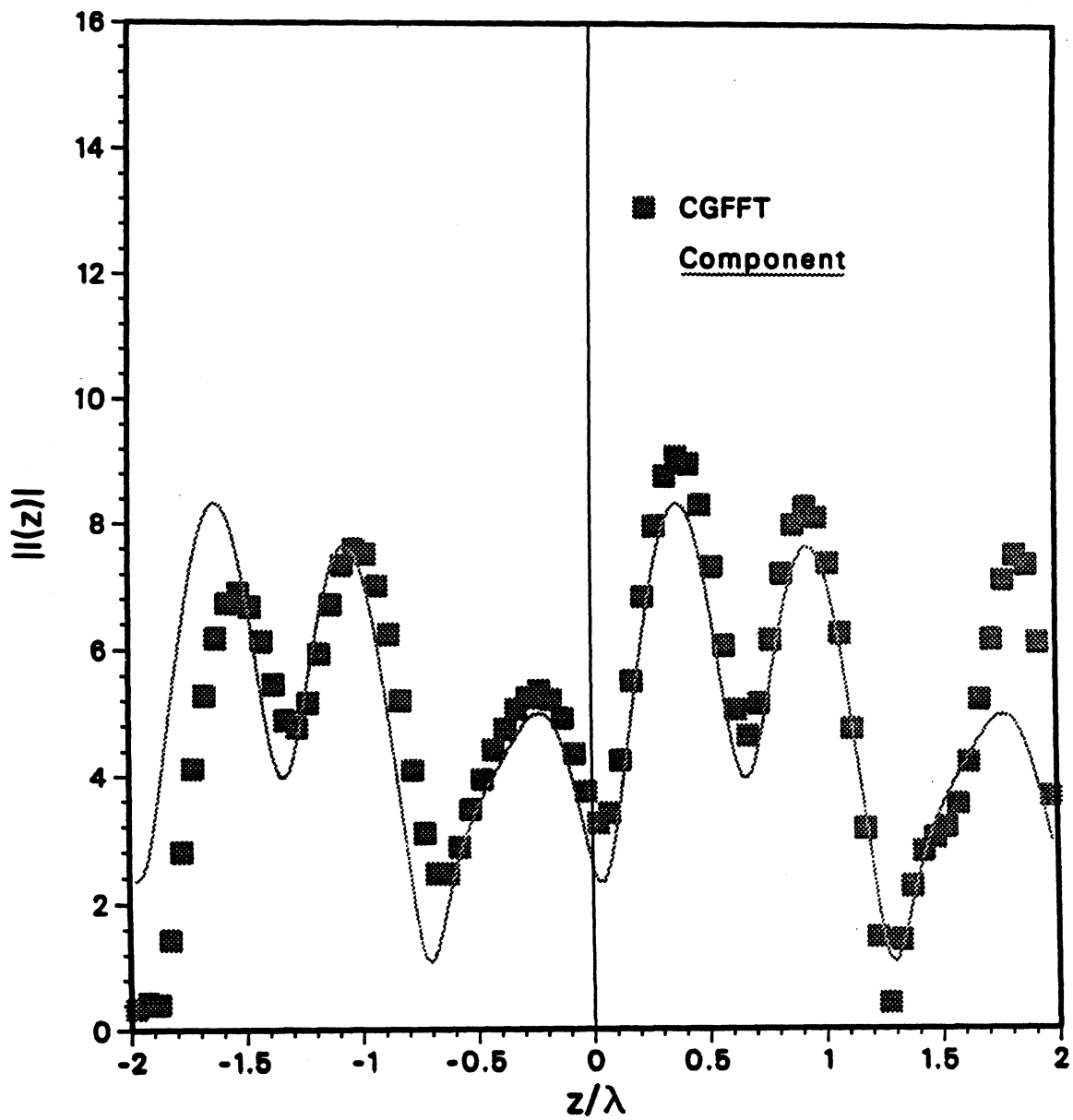
Figure 3.   H-polarization, side edge current on edge 2
of the plate, $\theta' = 60°$, W=2λ, L =4λ.
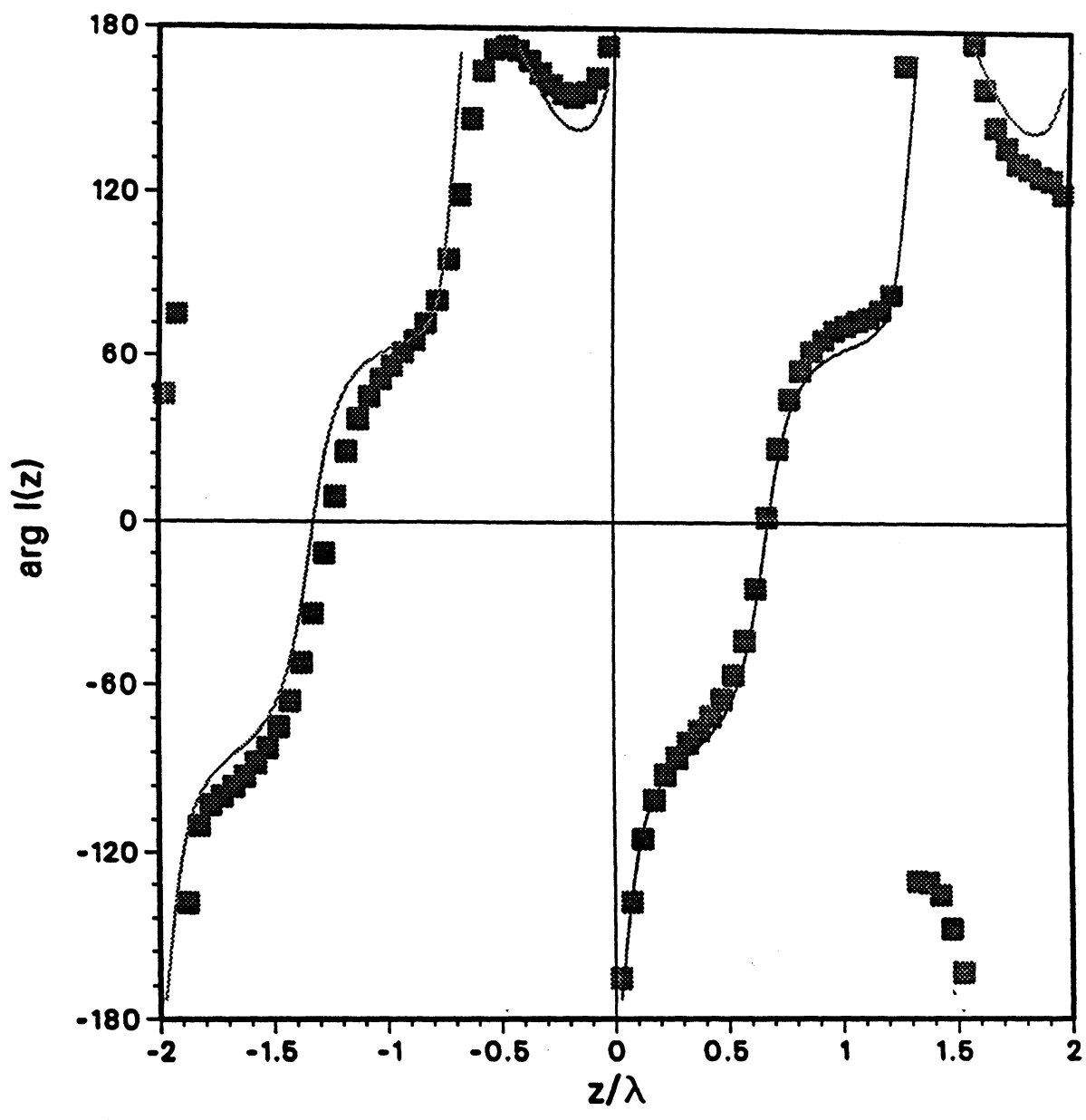
Figure 3b.   H-polarization, side edge current on edge 2
of the plate, $\theta' = 60°$, W=2λ, L=4λ.
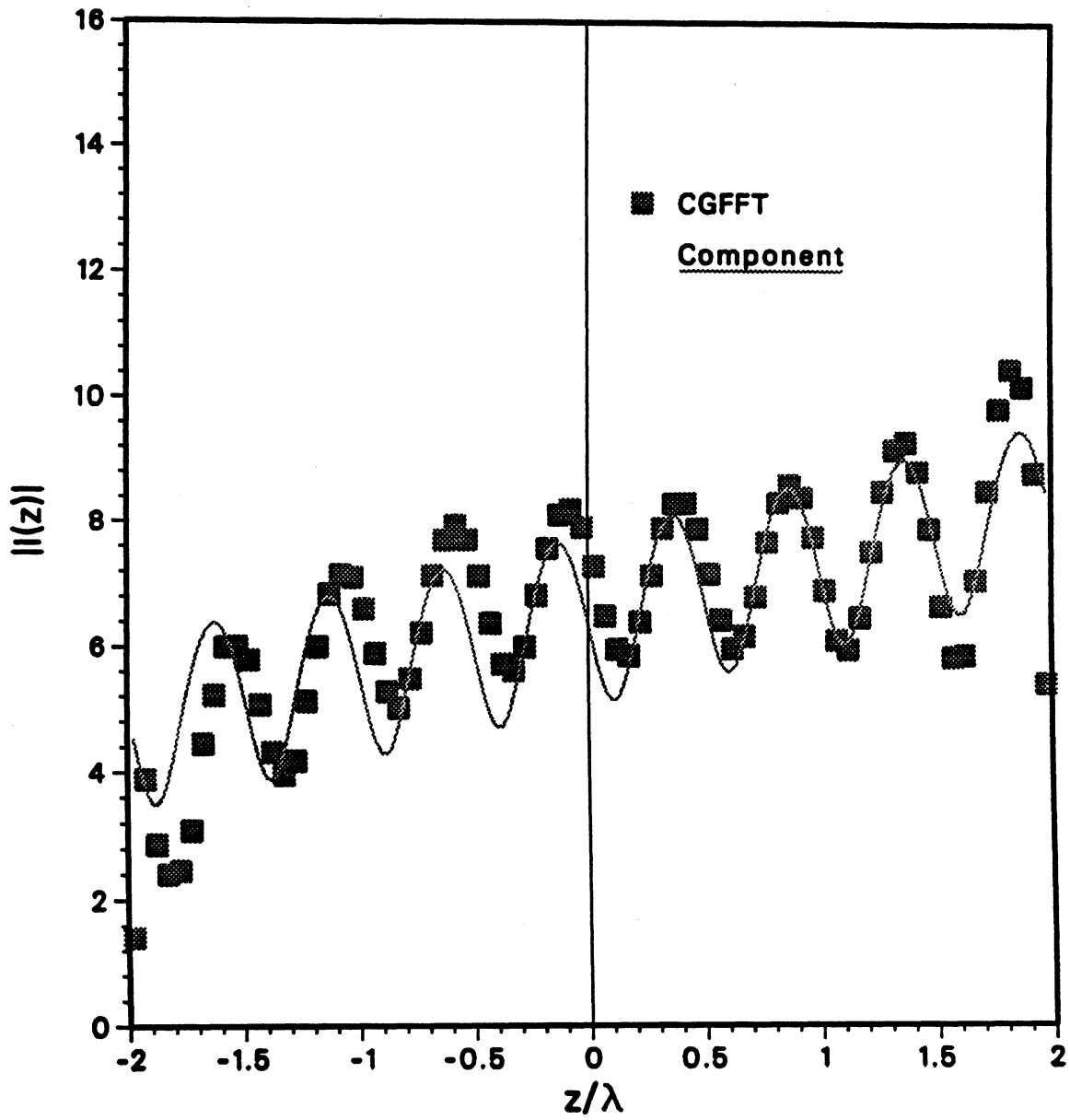
Figure 4.   E-polarization, side edge current on edge 2
            of the plate, $\theta' = 10°$, W=2λ, L =4λ.
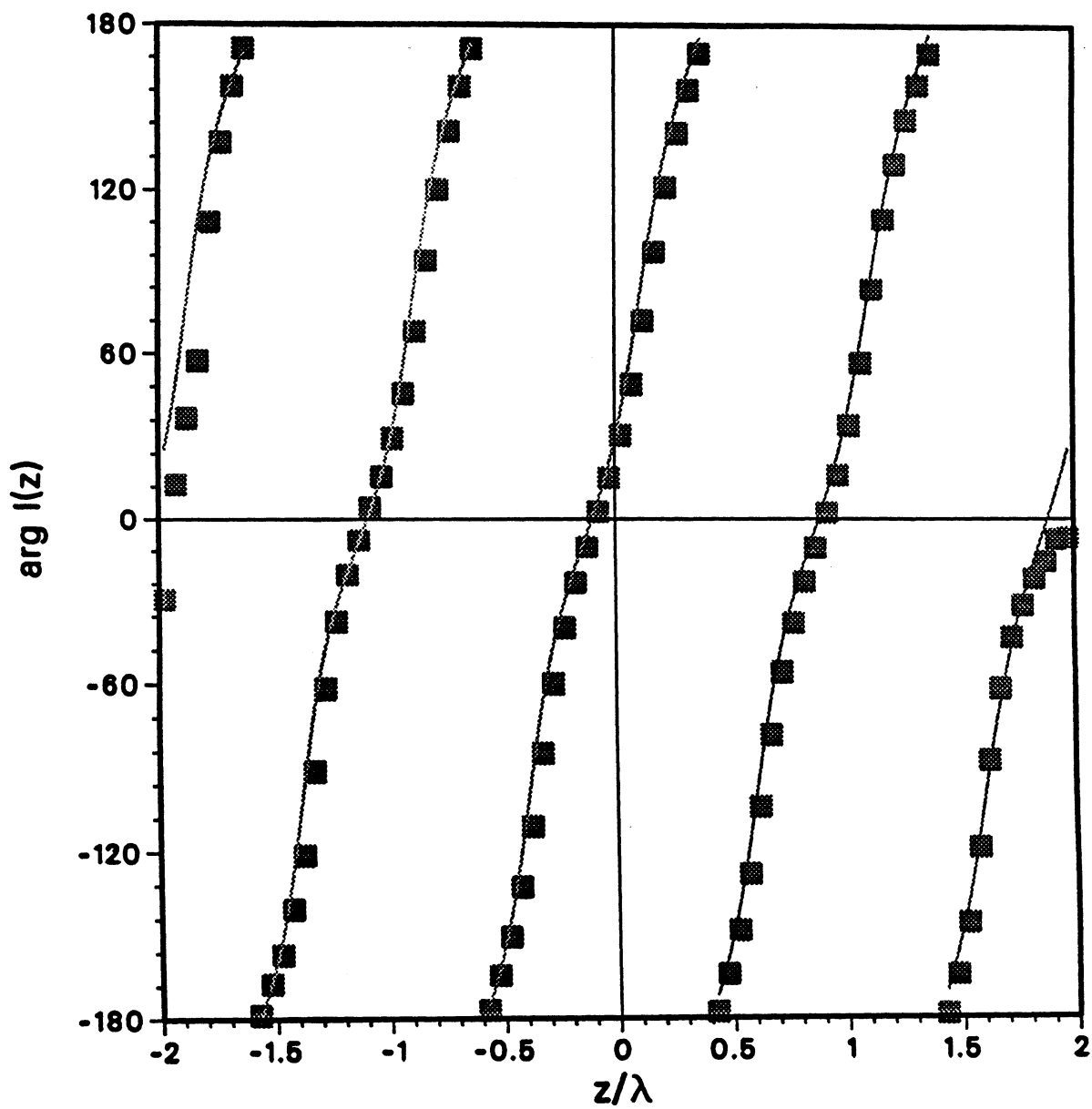
Figure 4b. E-polarization, side edge current on edge 2
of the plate, $\theta' = 10°$, W=2λ, L=4λ.
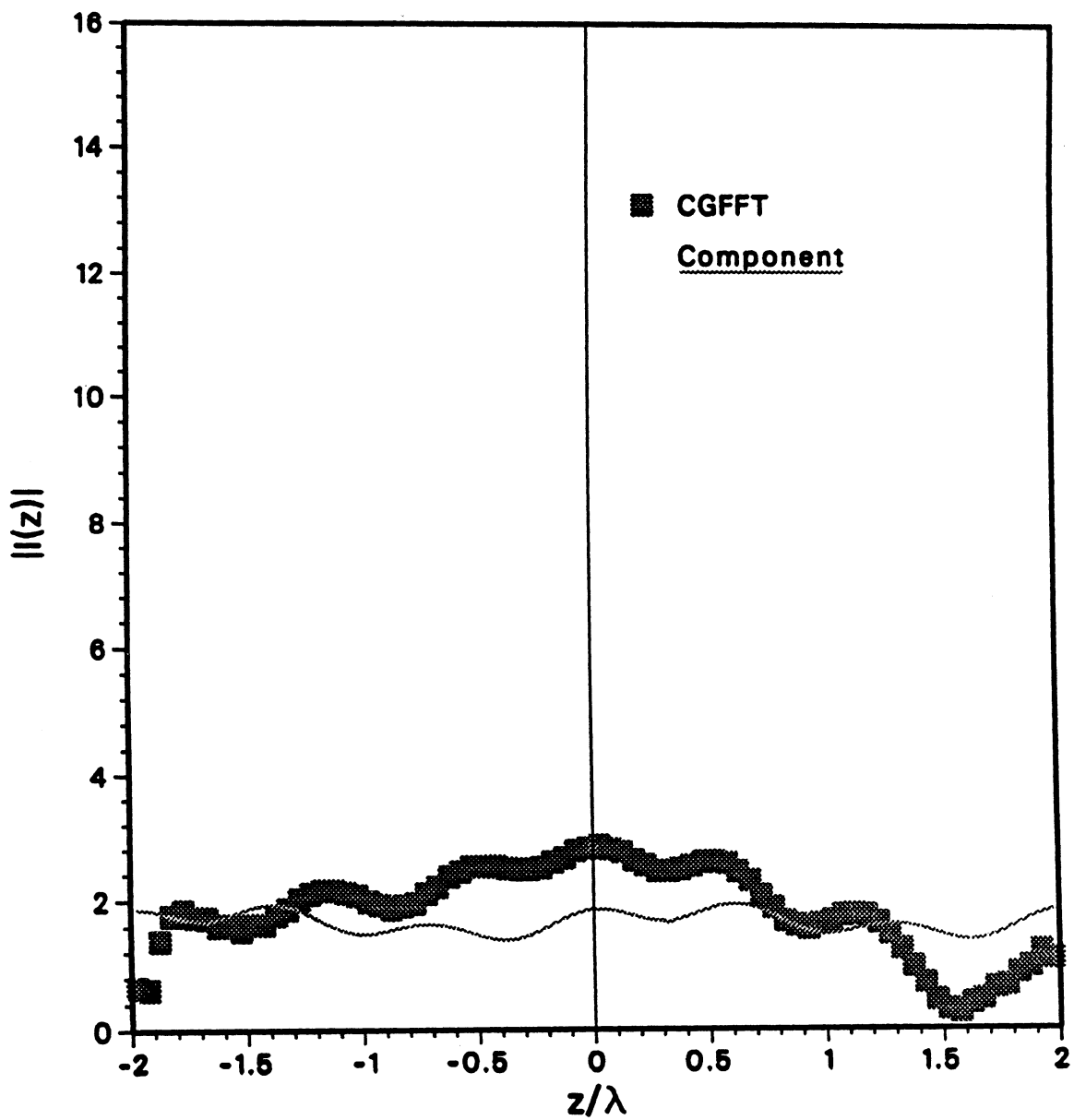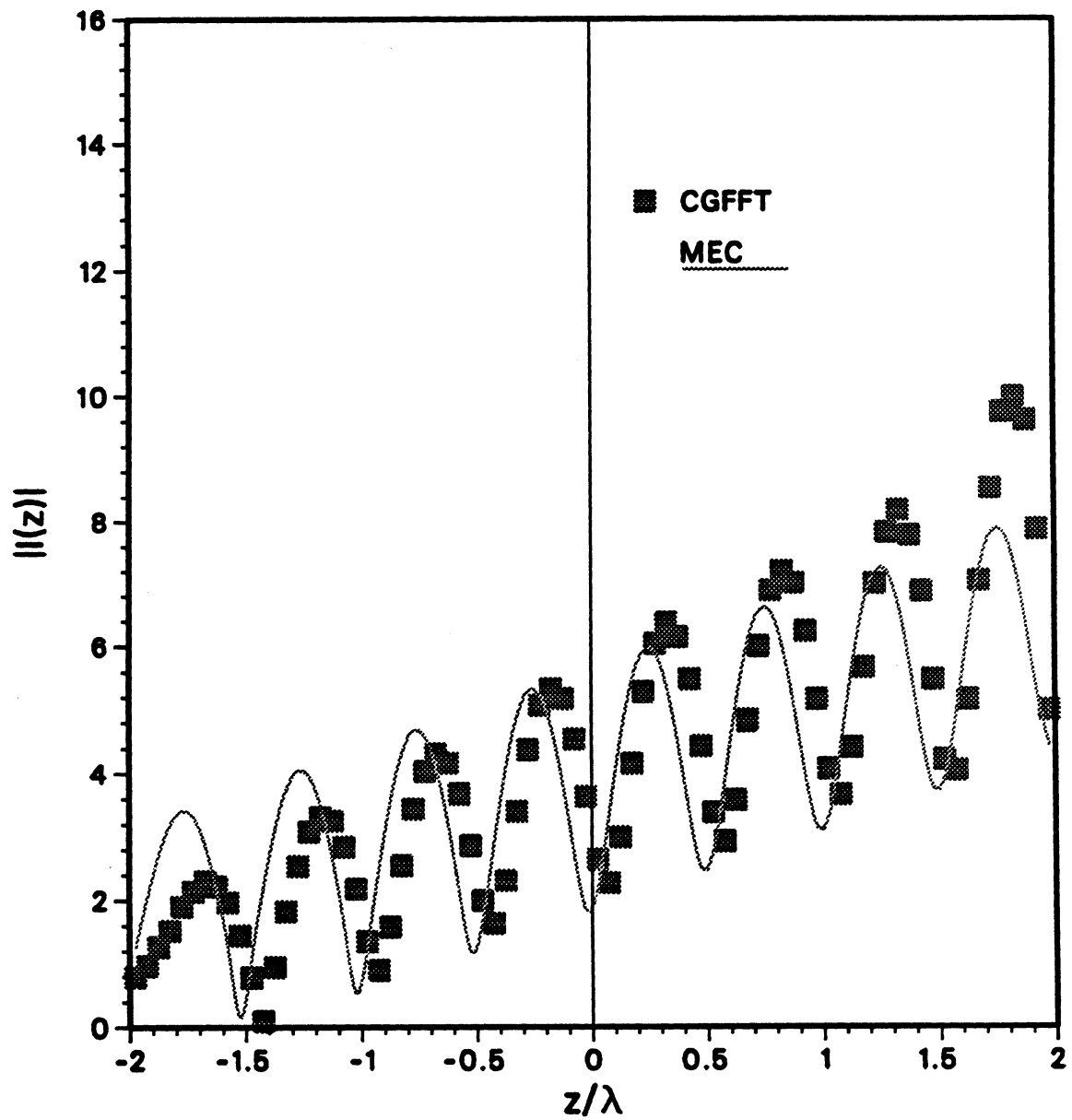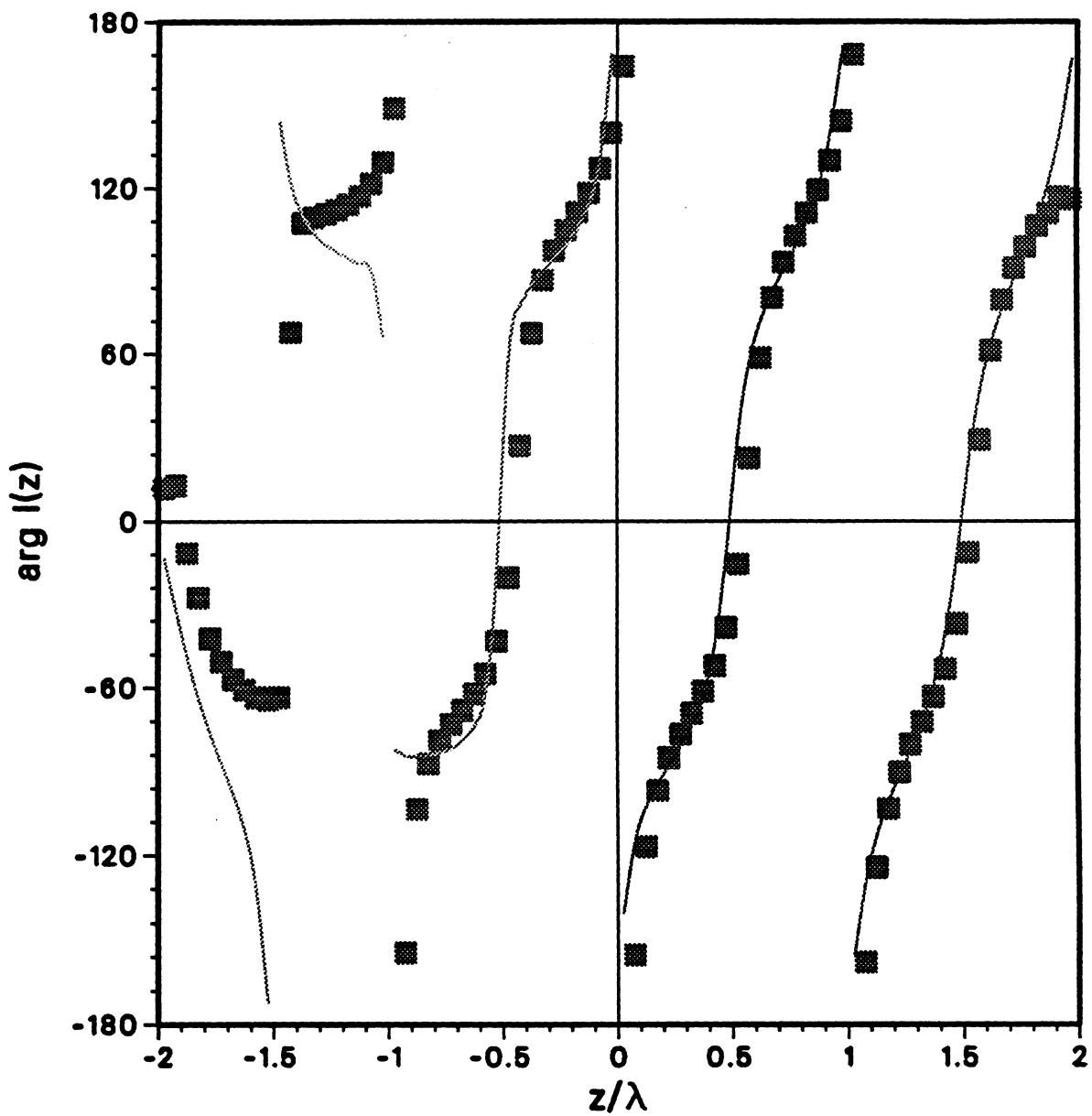
Figure 5.   E-polarization, side edge current on edge 2
of the plate, $\theta' = 60°$, W=2λ, L =4λ.
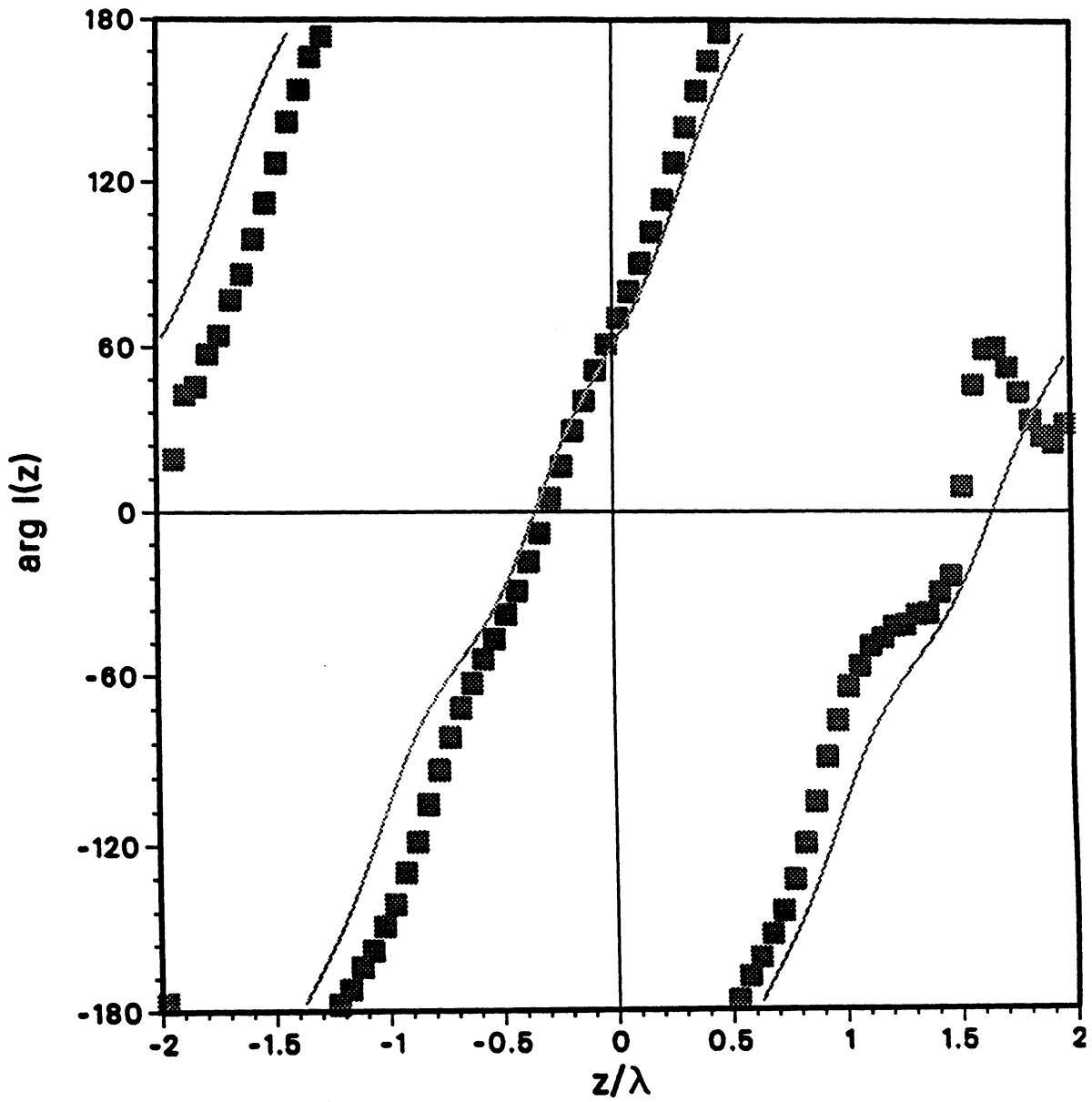
Figure 5b. E-polarization, side edge current on edge 2
of the plate, $\theta' = 60°$, W=2λ, L=4λ.
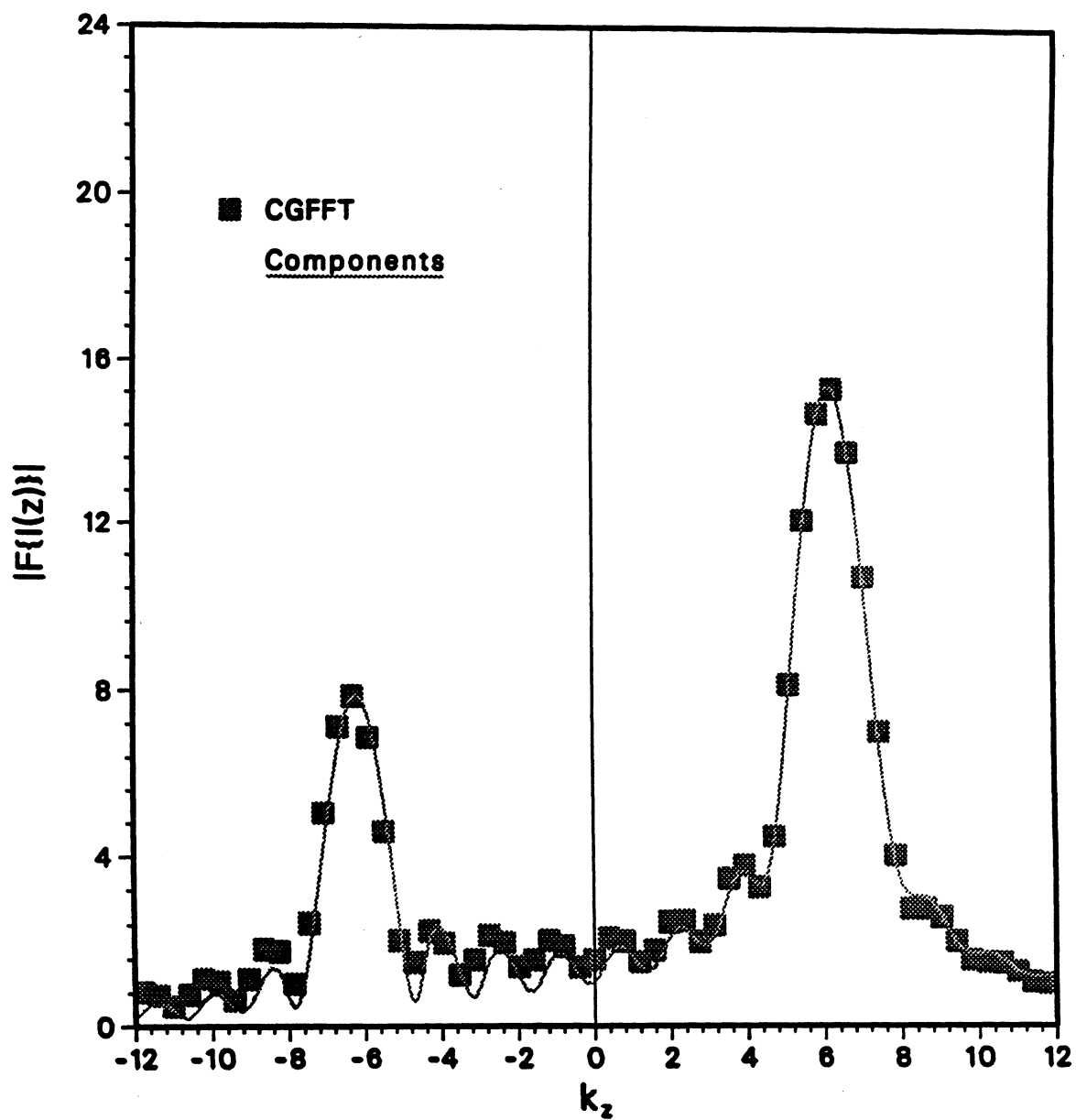
Figure 6.   H-polarization, Fourier transform of the current
on edge 2, $\theta' = 10°$, W=2λ, L =4λ.
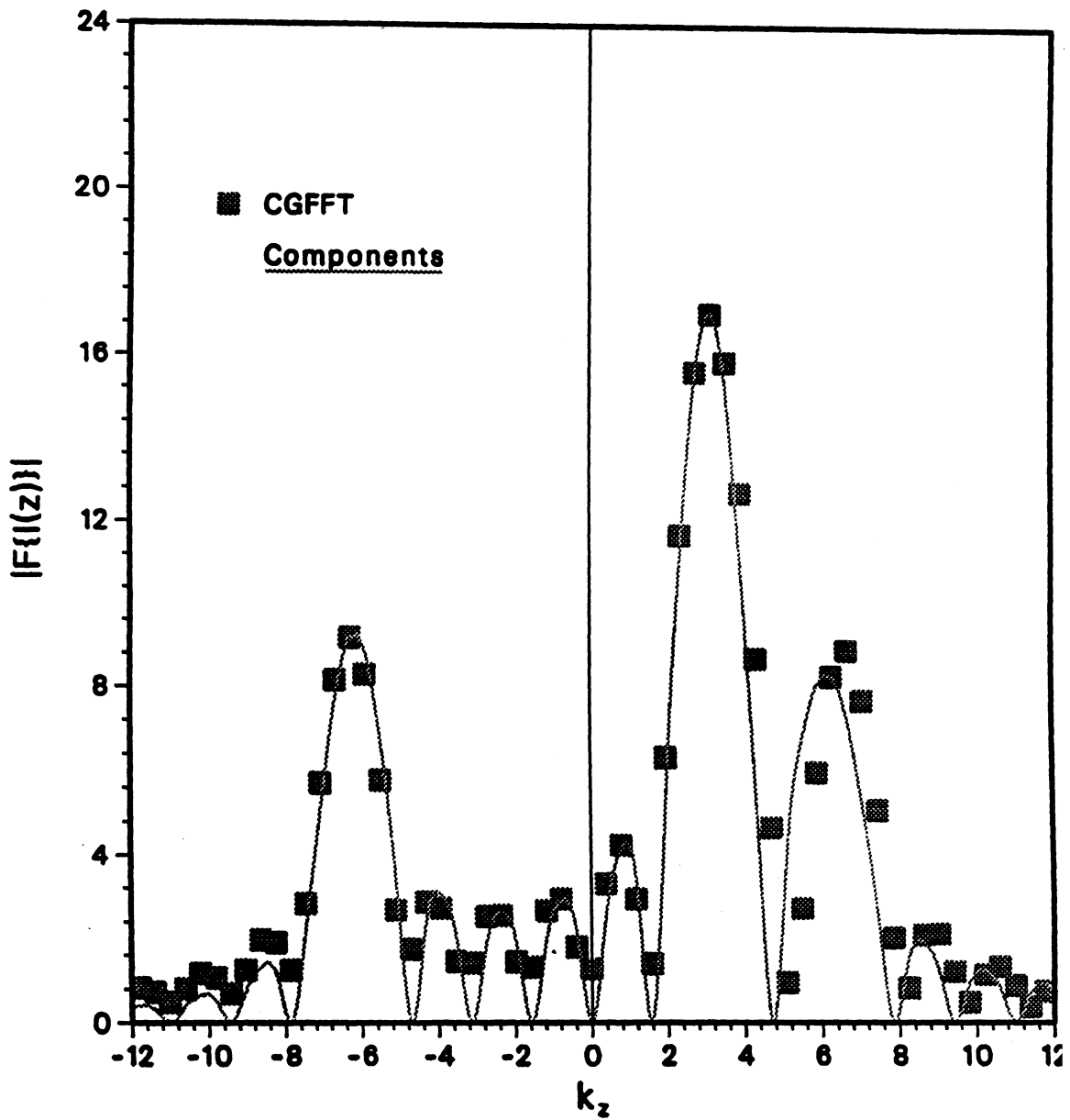
Figure 7.   H-polarization, Fourier transform of the current
on edge 2, $\theta'= 60°$, W$=2\lambda$, L $=4\lambda$.
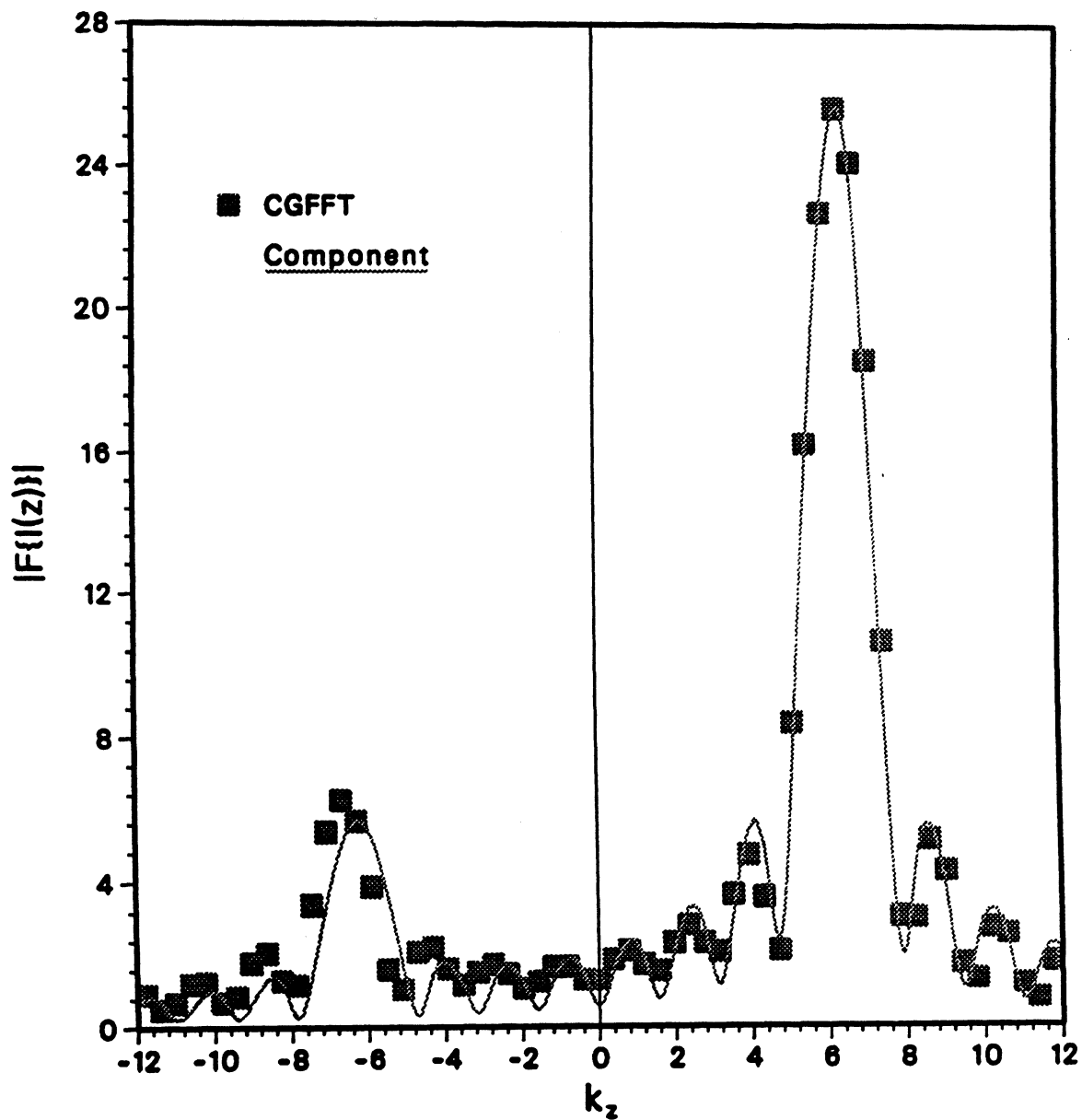
Figure 8.   E-polarization, Fourier transform of the current on edge 2, $\theta' = 10°$, W=2λ, L=4λ.
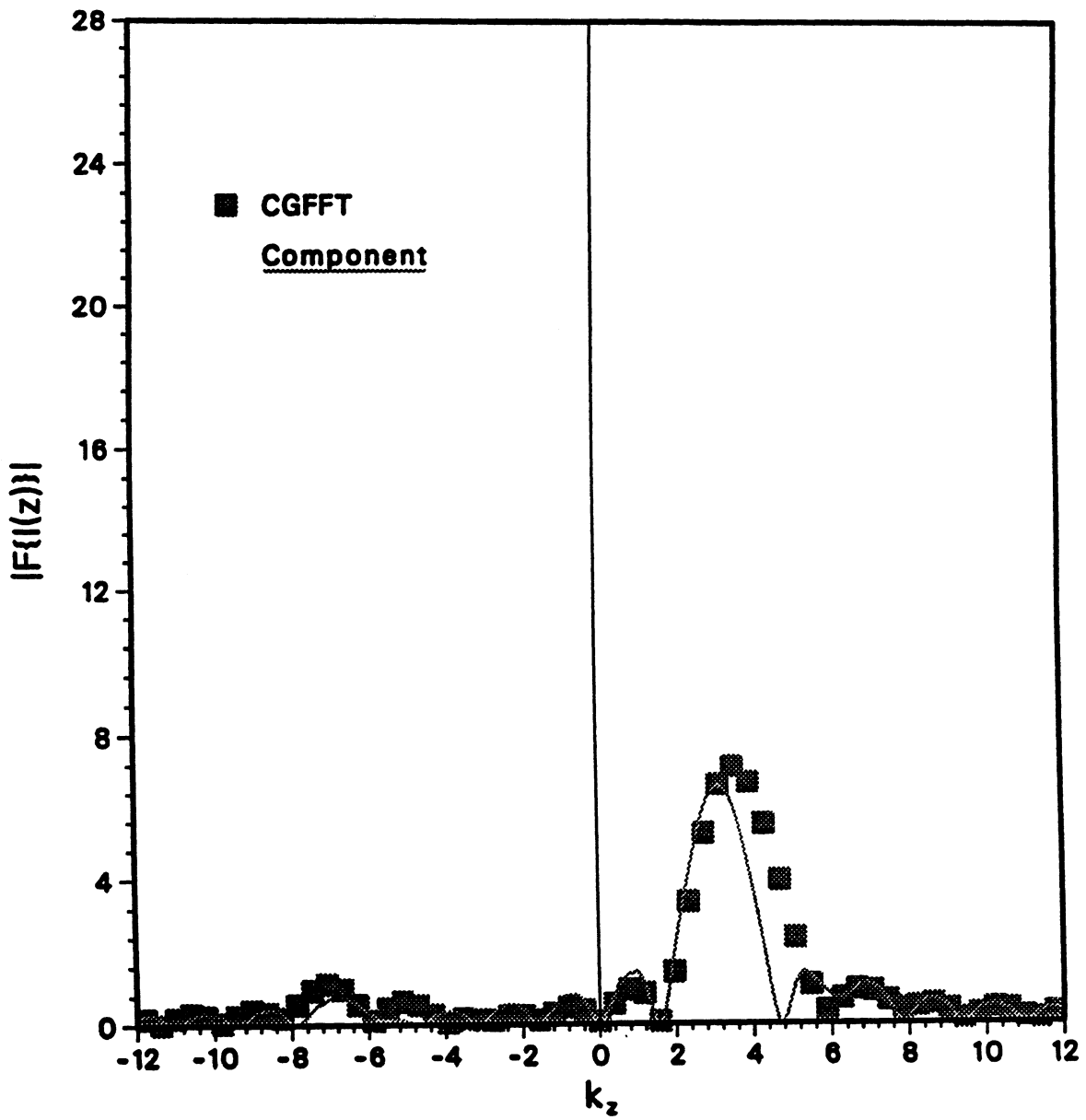
Figure 9. E-polarization, Fourier transform of the current on edge 2, $\theta' = 60°$, W=2λ, L=4λ.
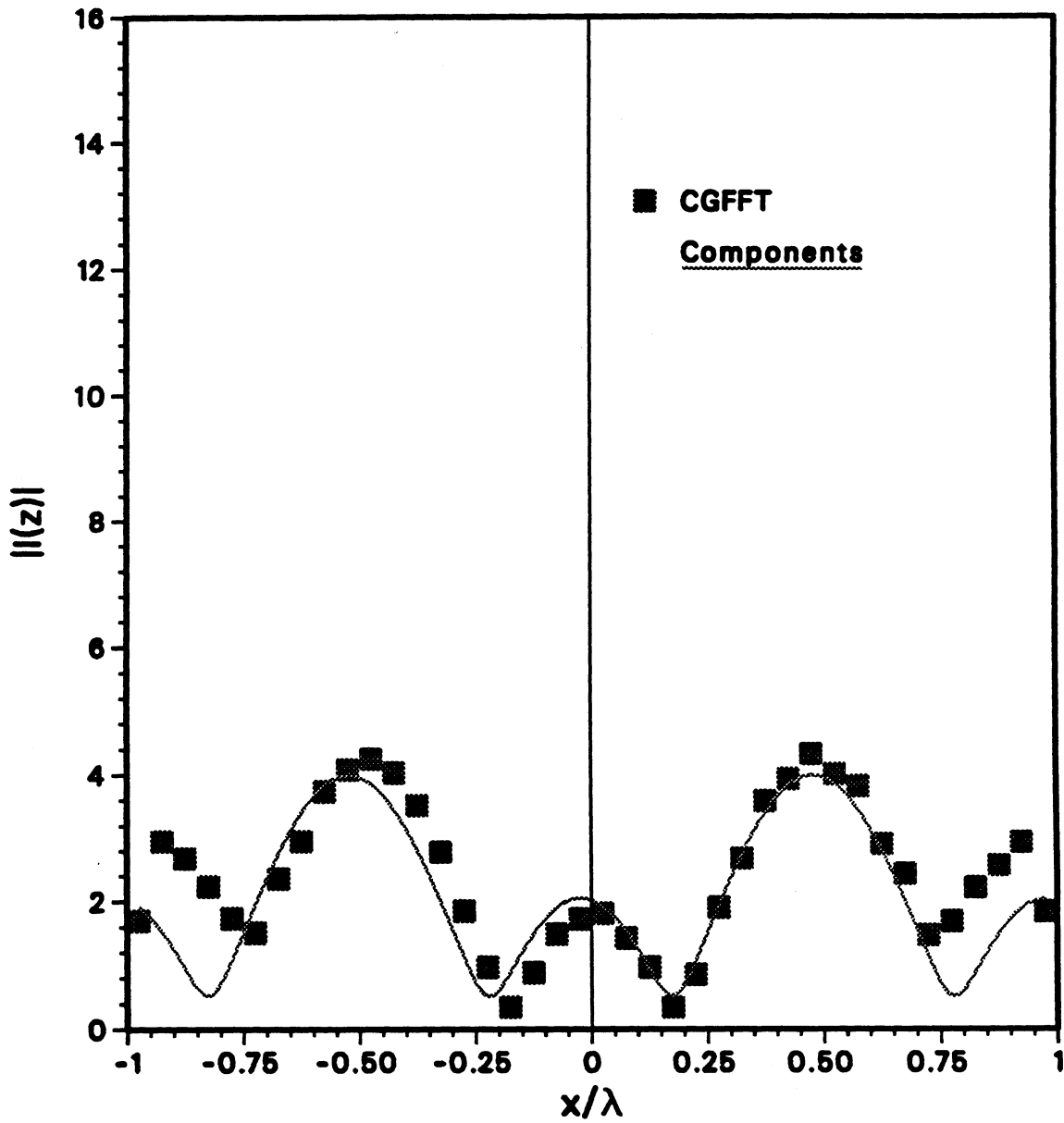
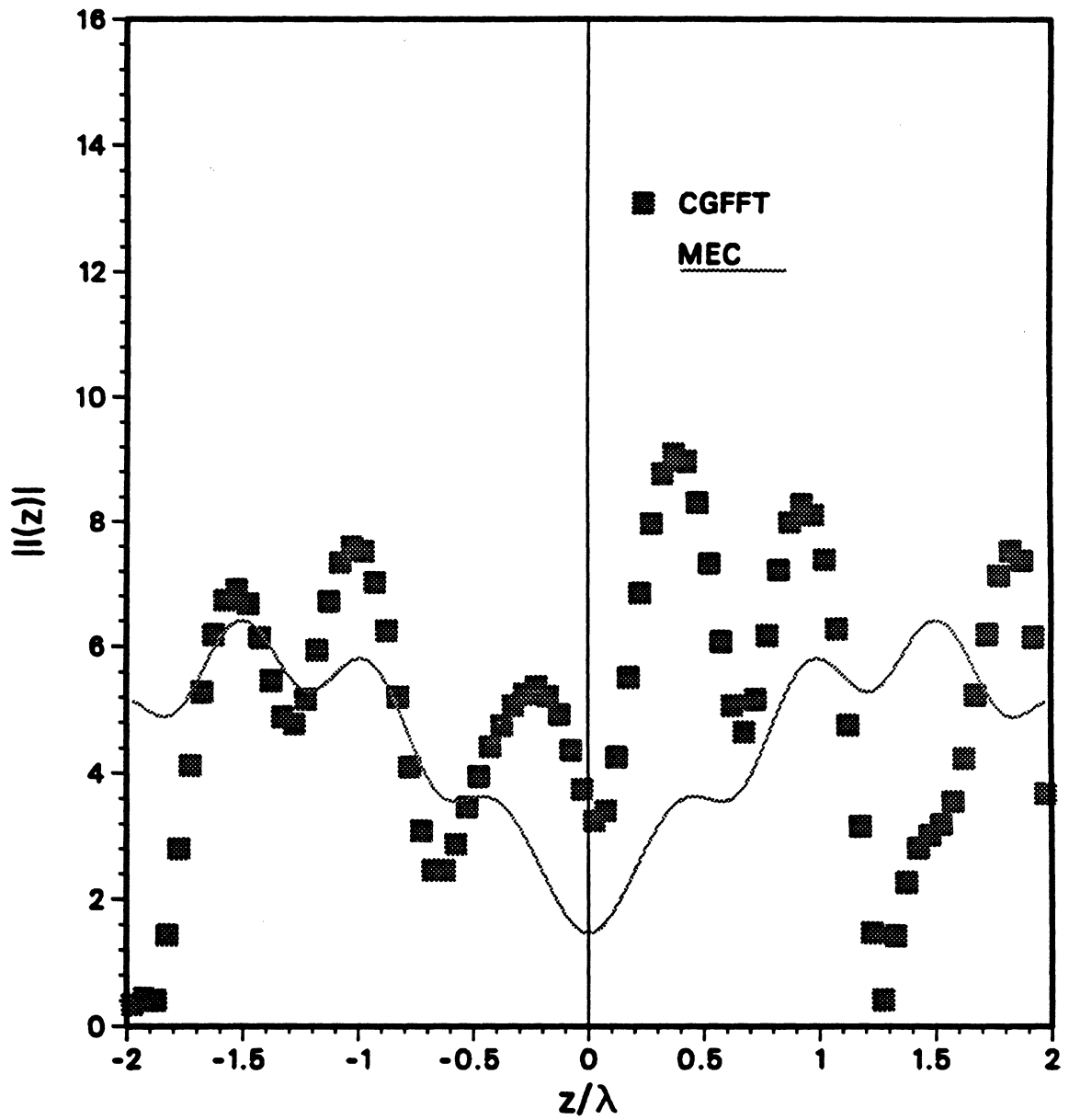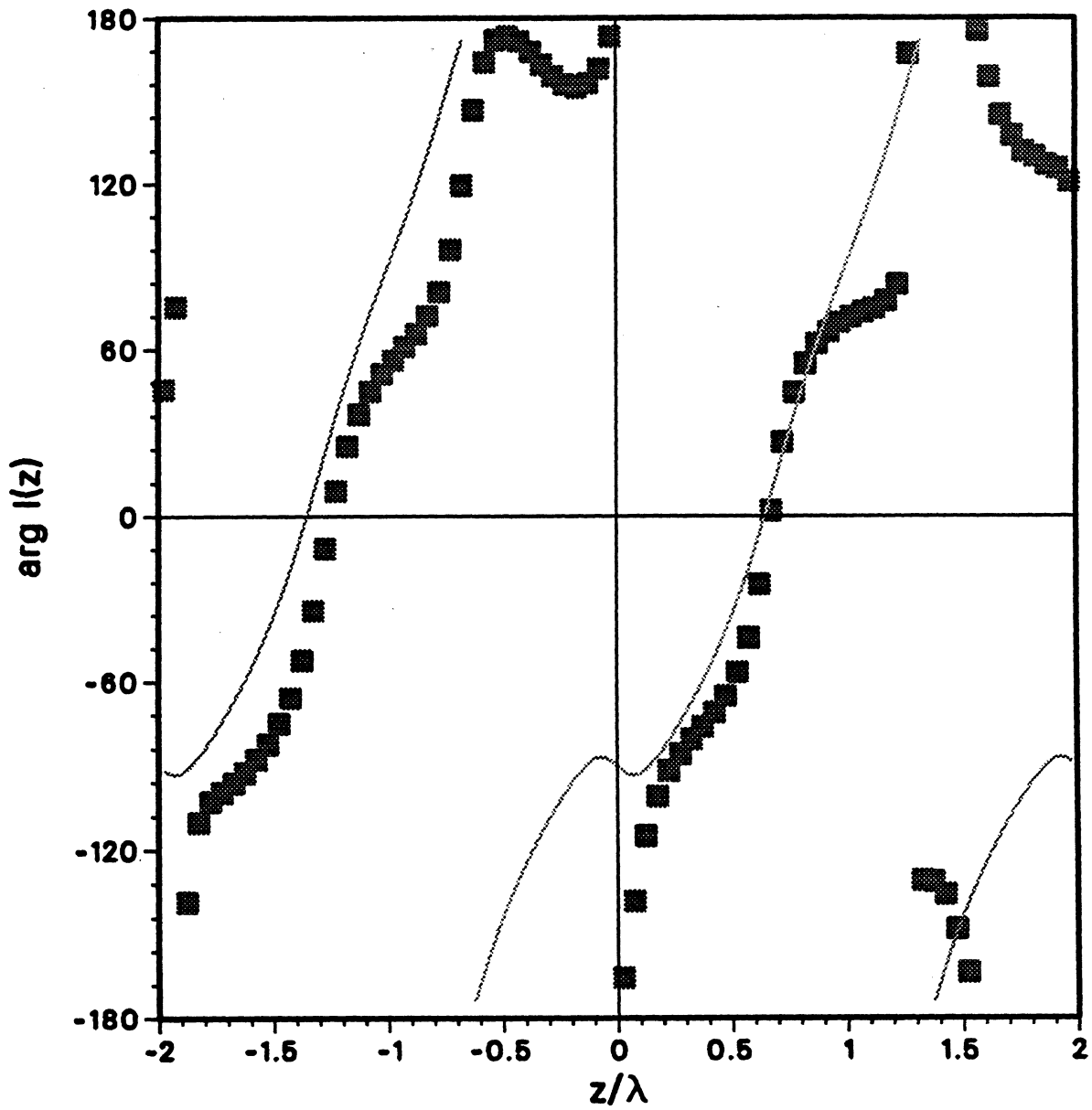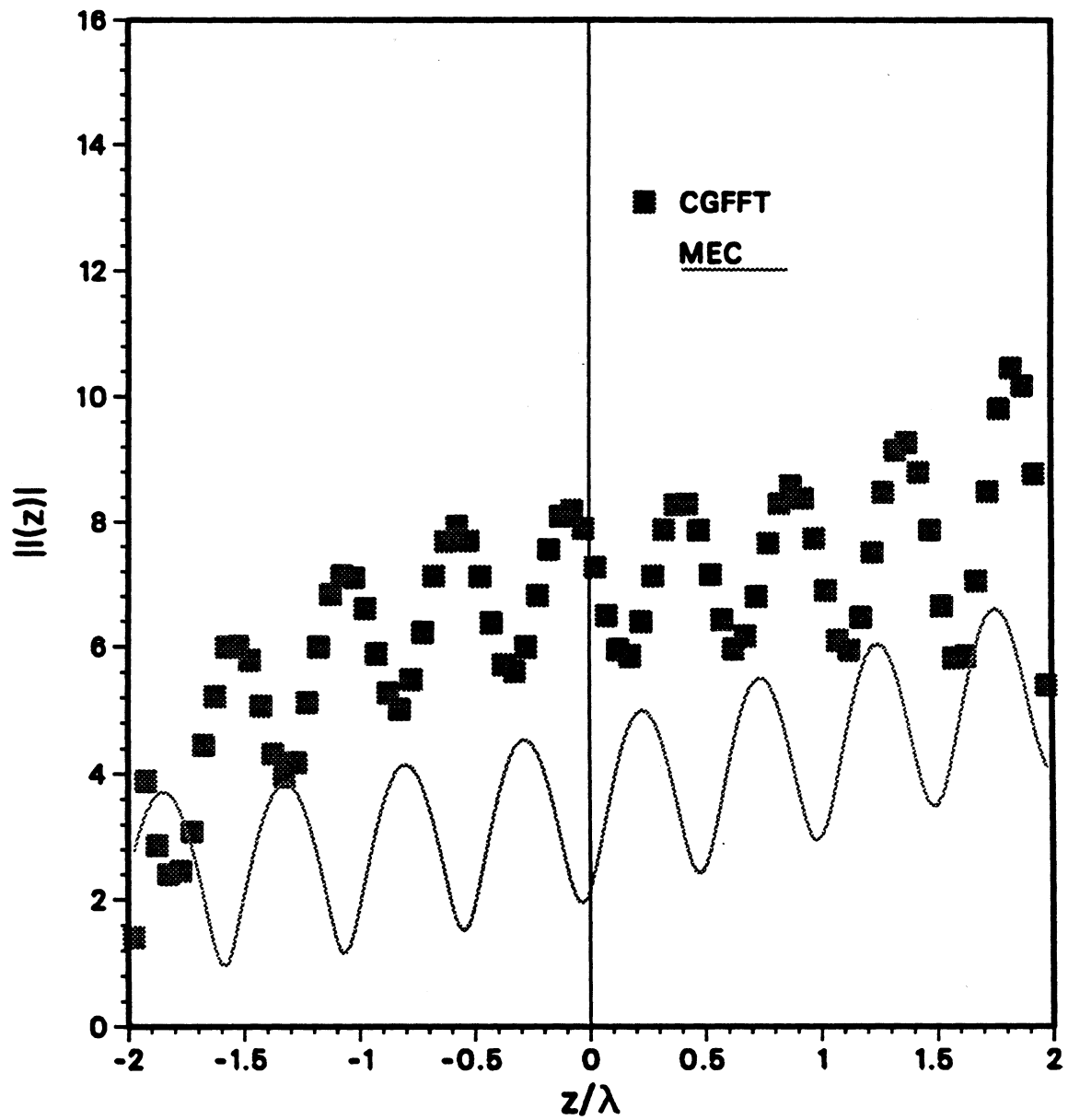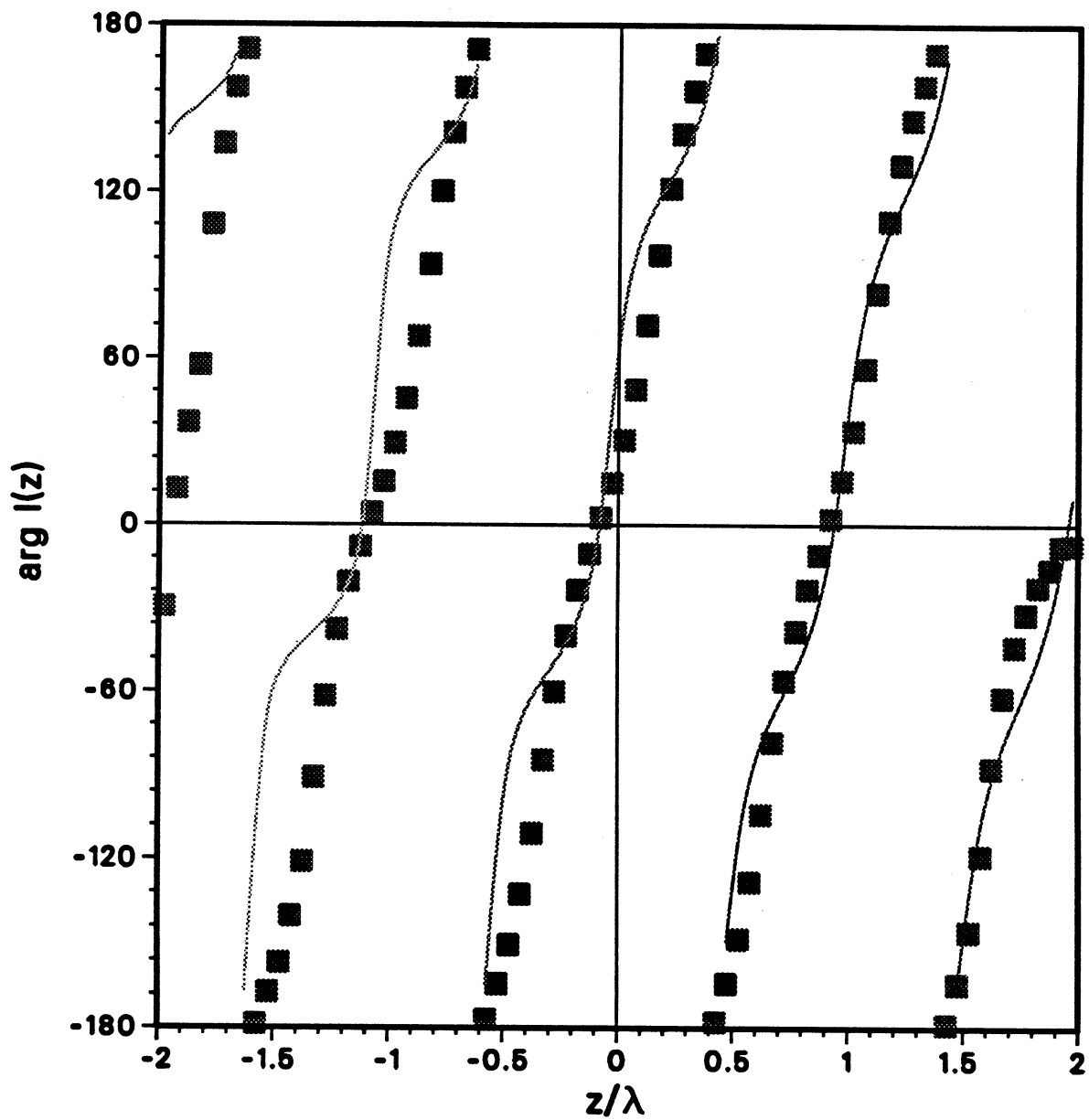Figure 10. E-polarization, current on edge 3 of the plate, $\theta' = 10°$, W=2λ, L=4λ.
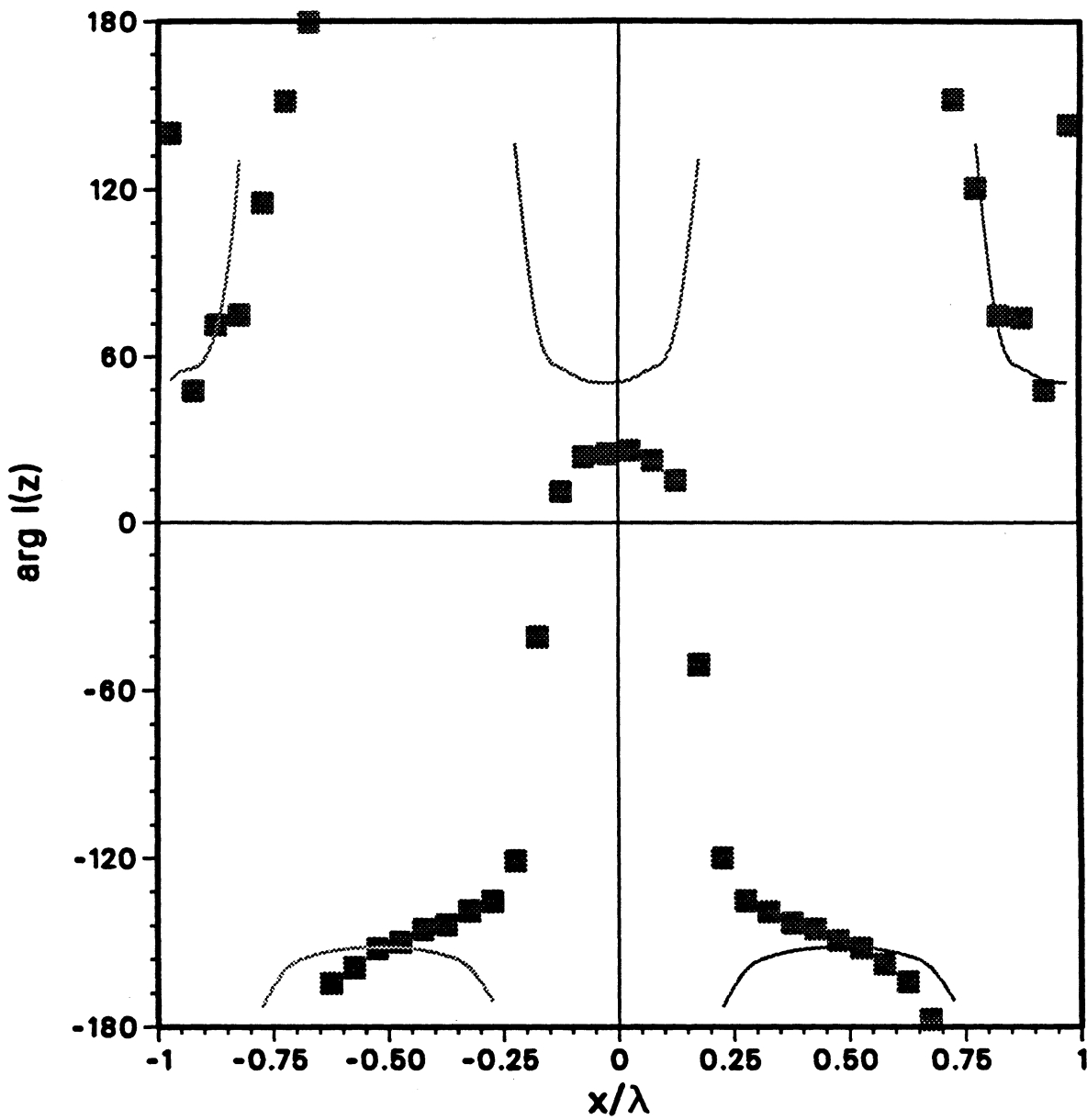
Figure 10b. E-polarization, current on edge 2
of the plate, $\theta' = 10°$, W=2λ, L=4λ.
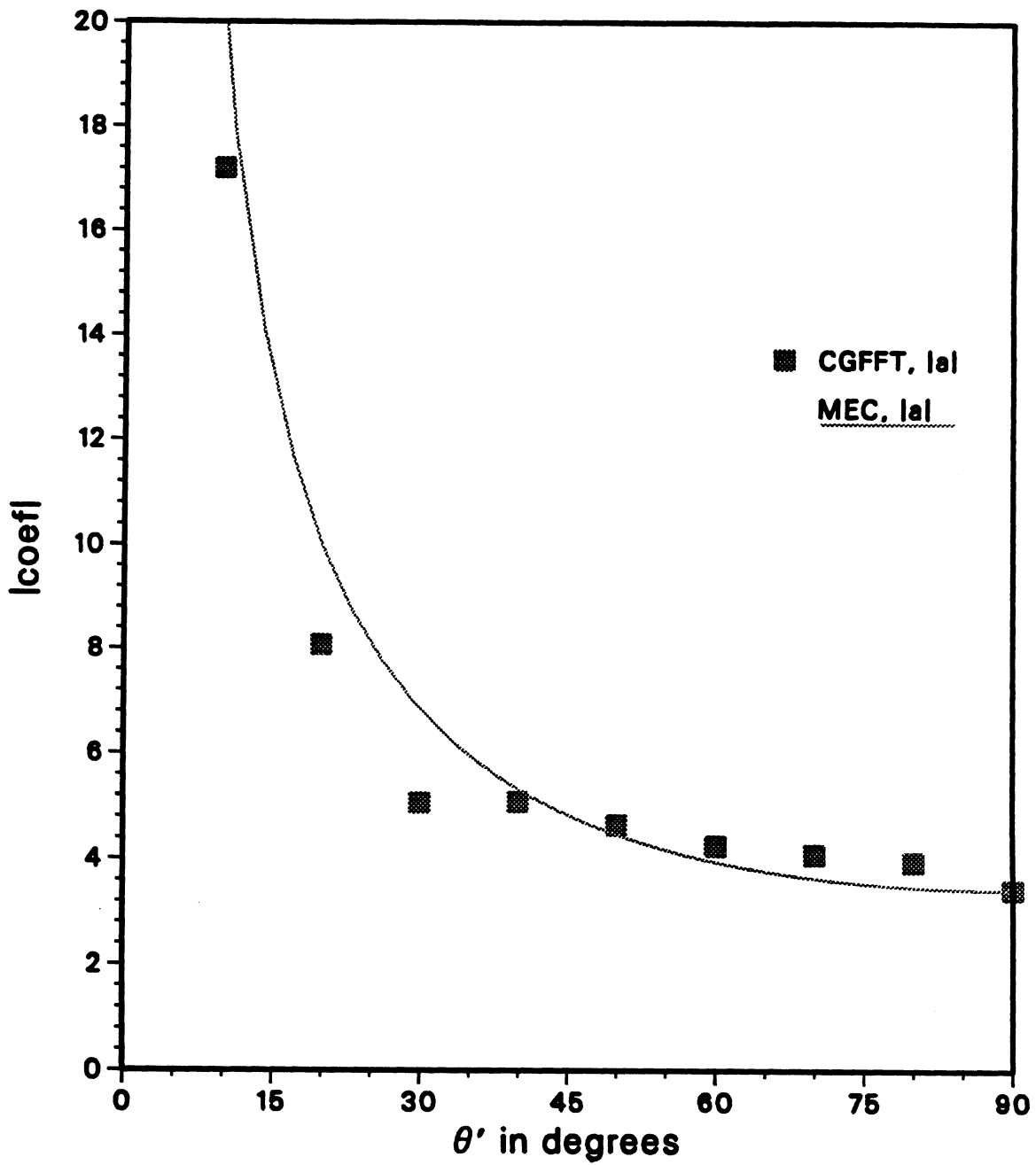
Figure 11. H-polarization, coefficient a(θ')

for edge 2 of the plate, W=2λ, L=4λ.

Figure 11b. H-polarization, coefficient a(θ')

for edge 2 of the plate, W=2λ, L=4λ.

Figure 12.   H-polarization, coefficient b(θ')

for edge 2 of the plate, W=2λ, L=4λ.
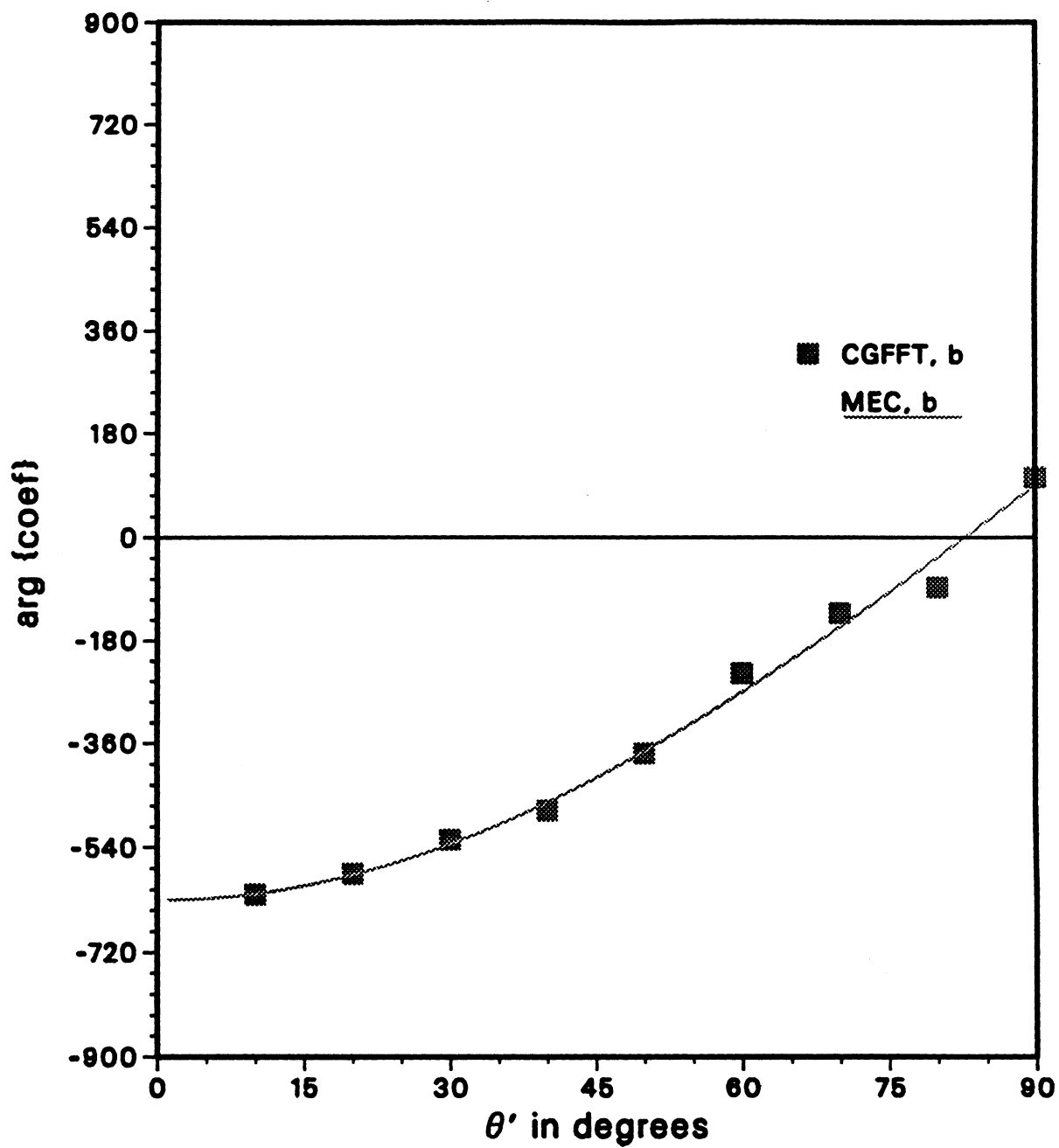
Figure 12b. H-polarization, coefficient b(θ')

for edge 2 of the plate, W=2λ, L=4λ.
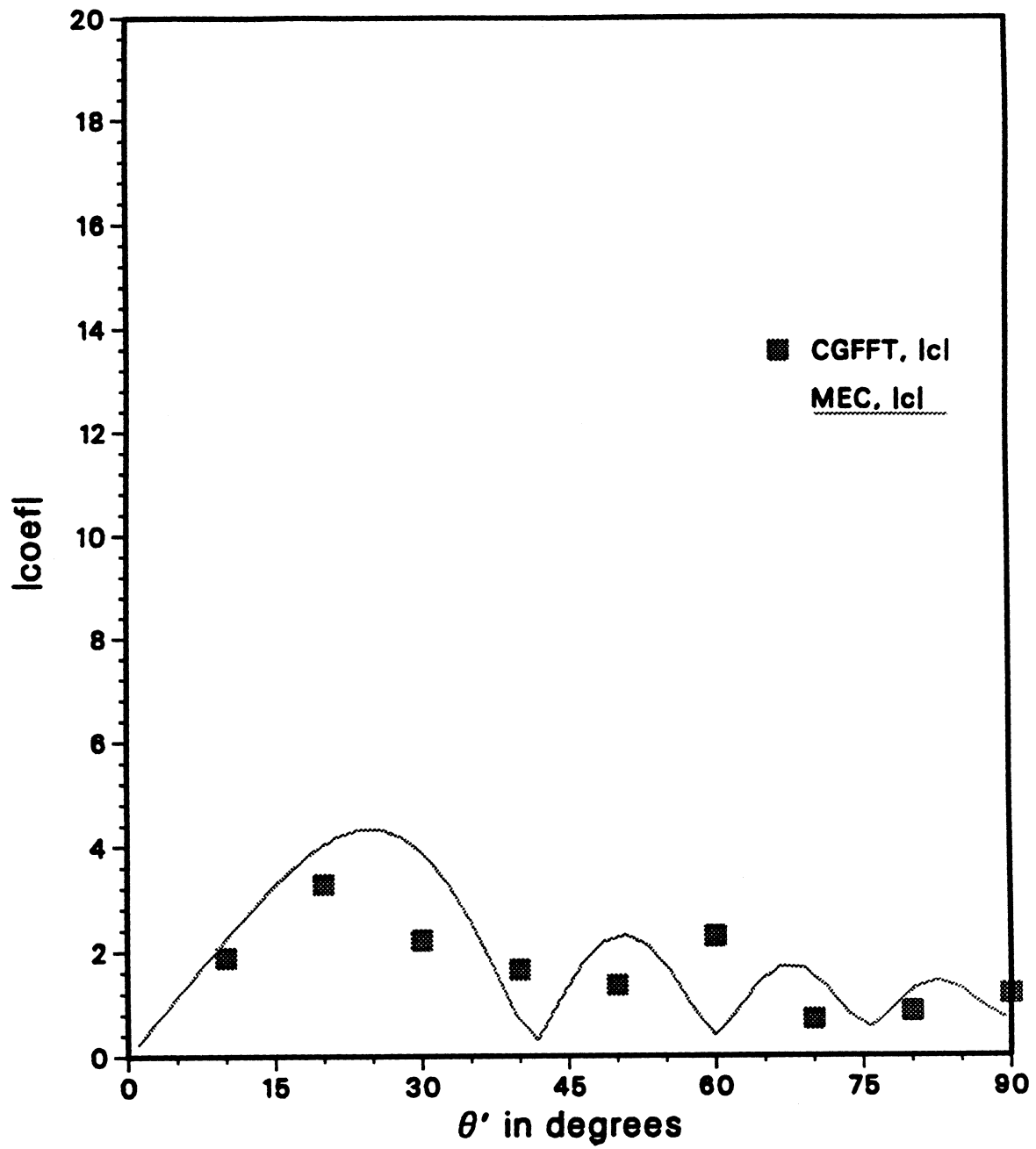
Figure 13. H-polarization, coefficient c(θ')

for edge 2 of the plate, W=2λ, L=4λ.
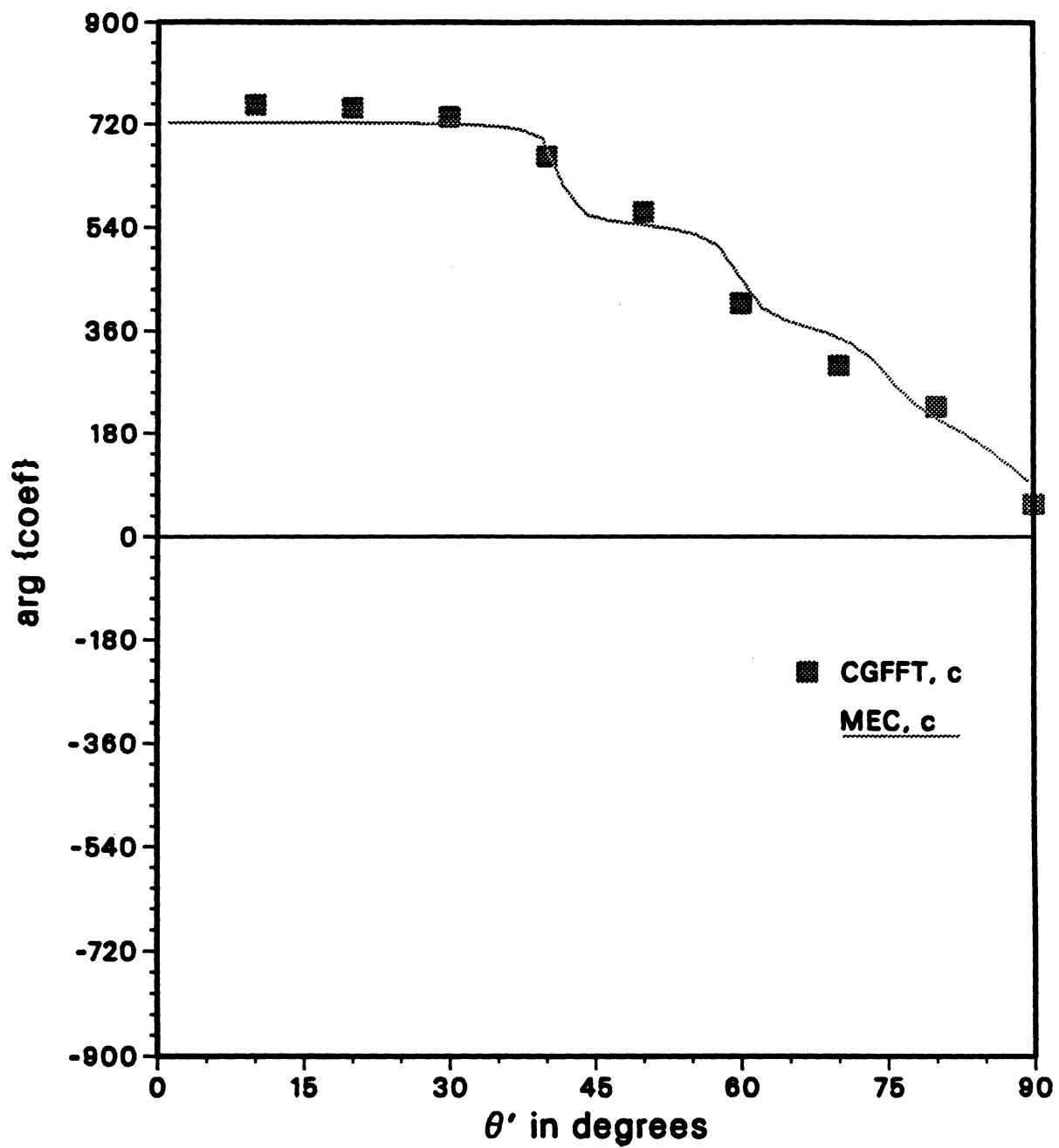
Figure 13b. H-polarization, coefficient c(θ')
for edge 2 of the plate, W=2λ, L=4λ.
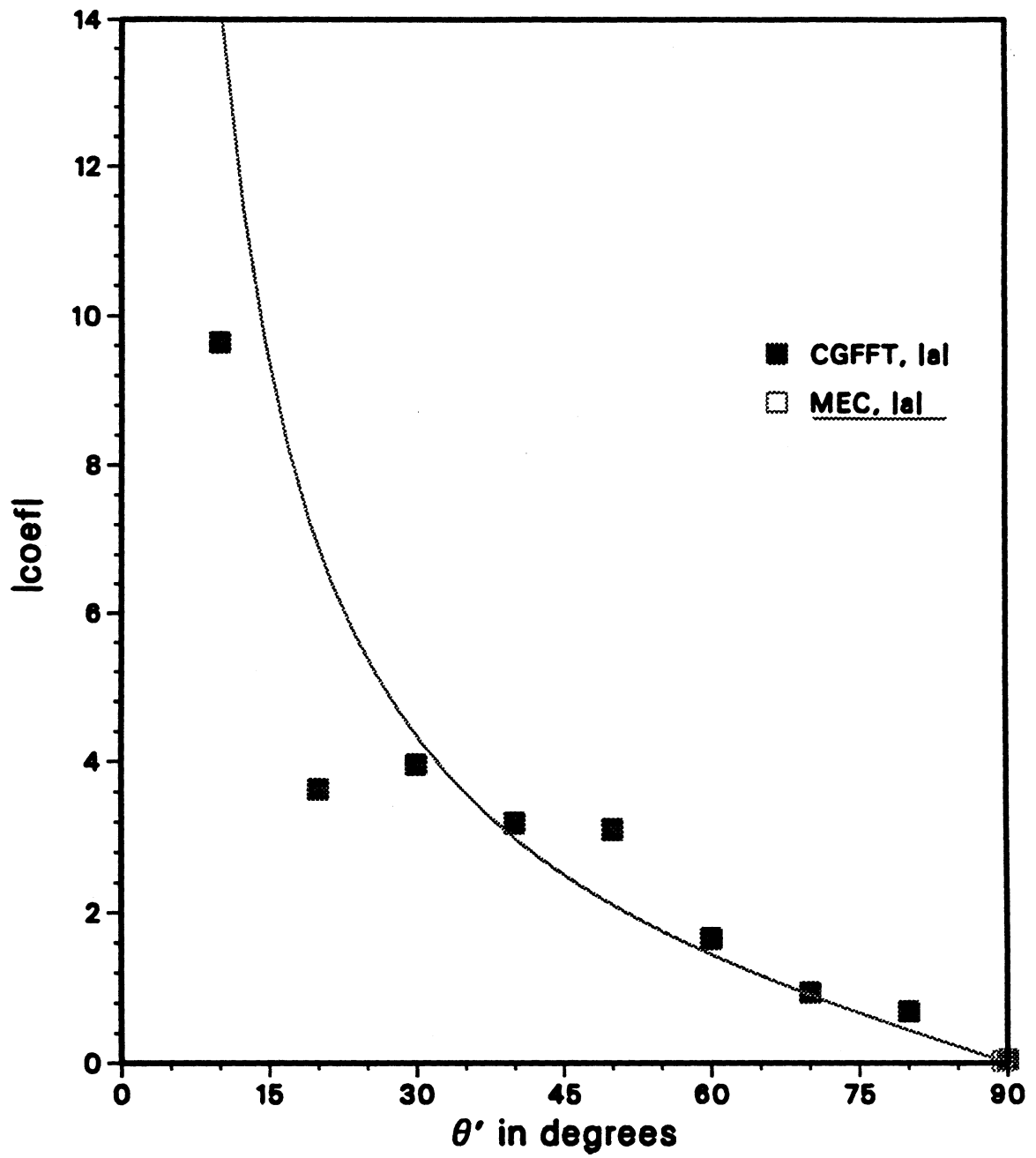
Figure 14.   E-polarization, coefficient a(θ')

for edge 2 of the plate, W=2λ, L=4λ.

Figure 14b. E-polarization, coefficient $a(\theta')$

for edge 2 of the plate, $W=2\lambda$, $L=4\lambda$.
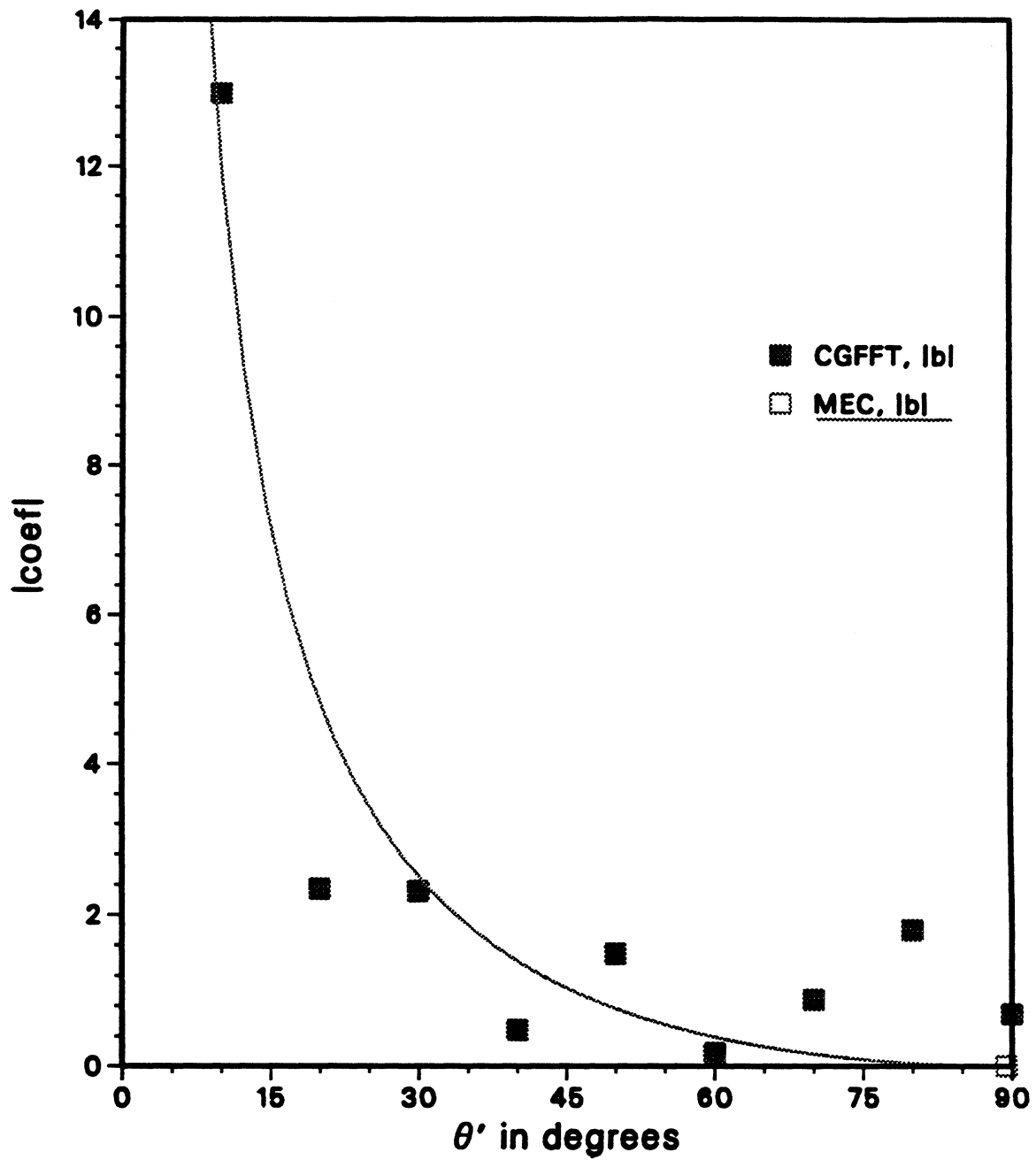
Figure 15.   E-polarization, coefficient b(θ')

for edge 2 of the plate, W=2λ, L=4λ.
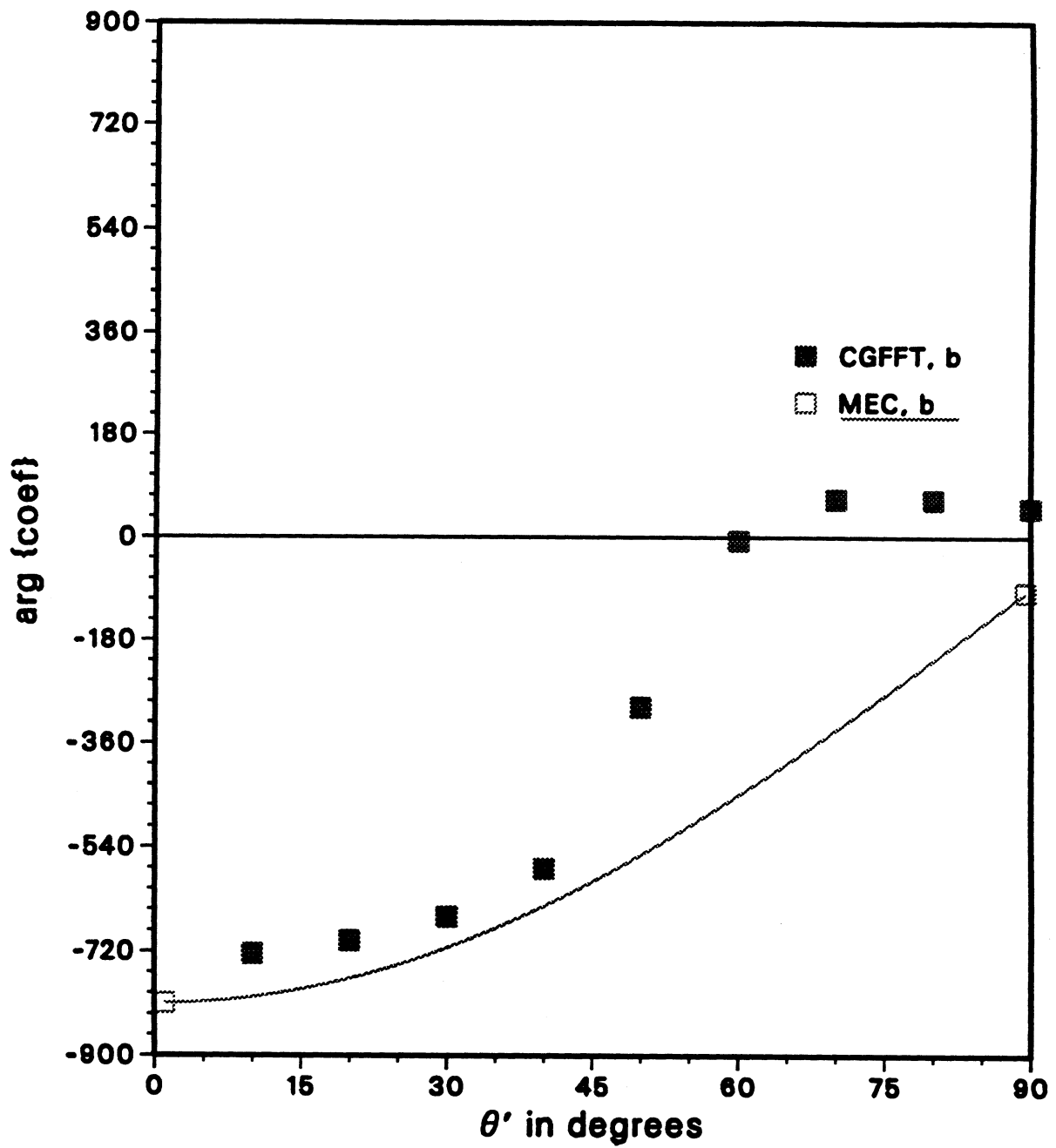
Figure 15b. E-polarization, coefficient b(θ')
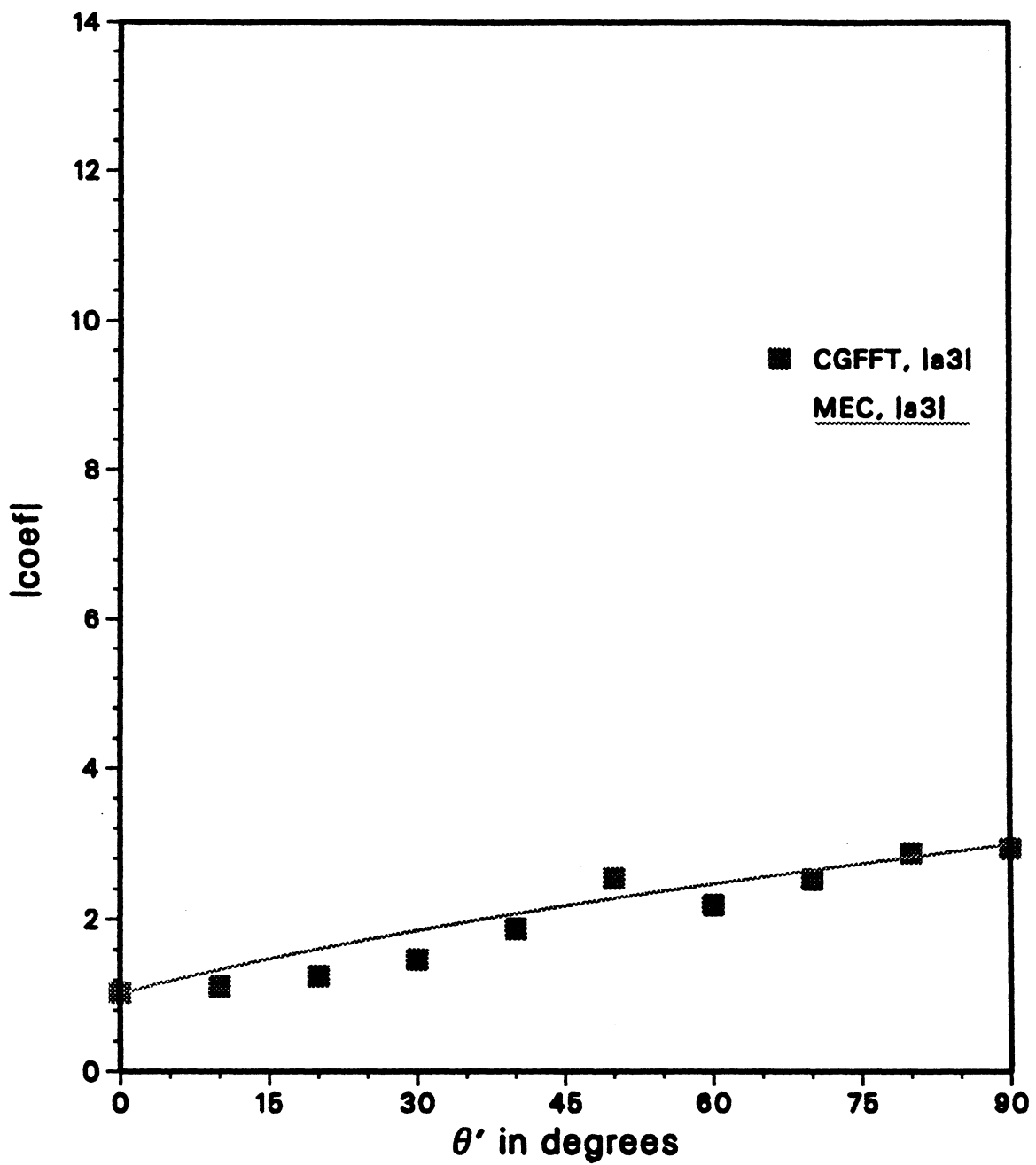
for edge 2 of the plate, W=2λ, L=4λ.
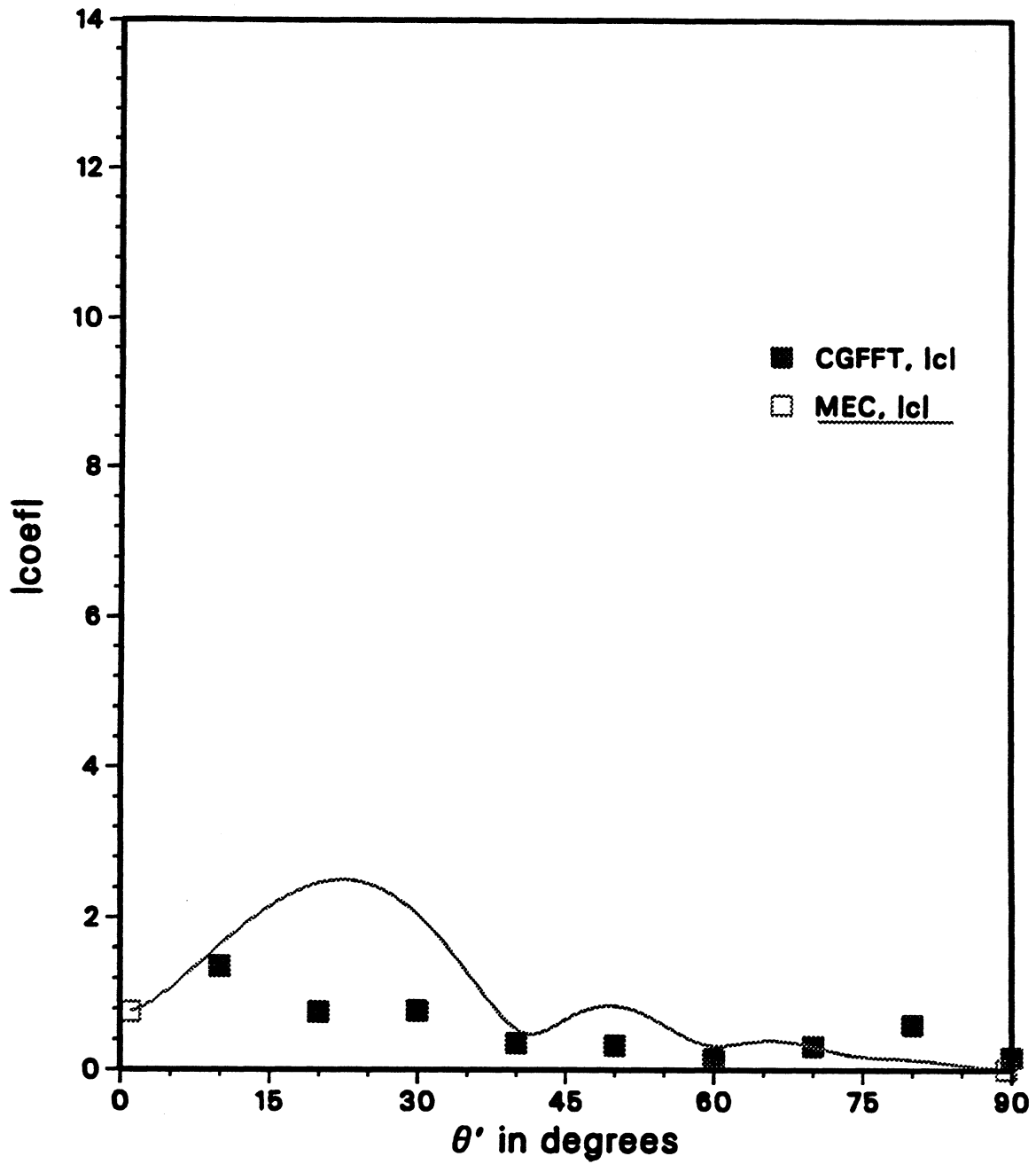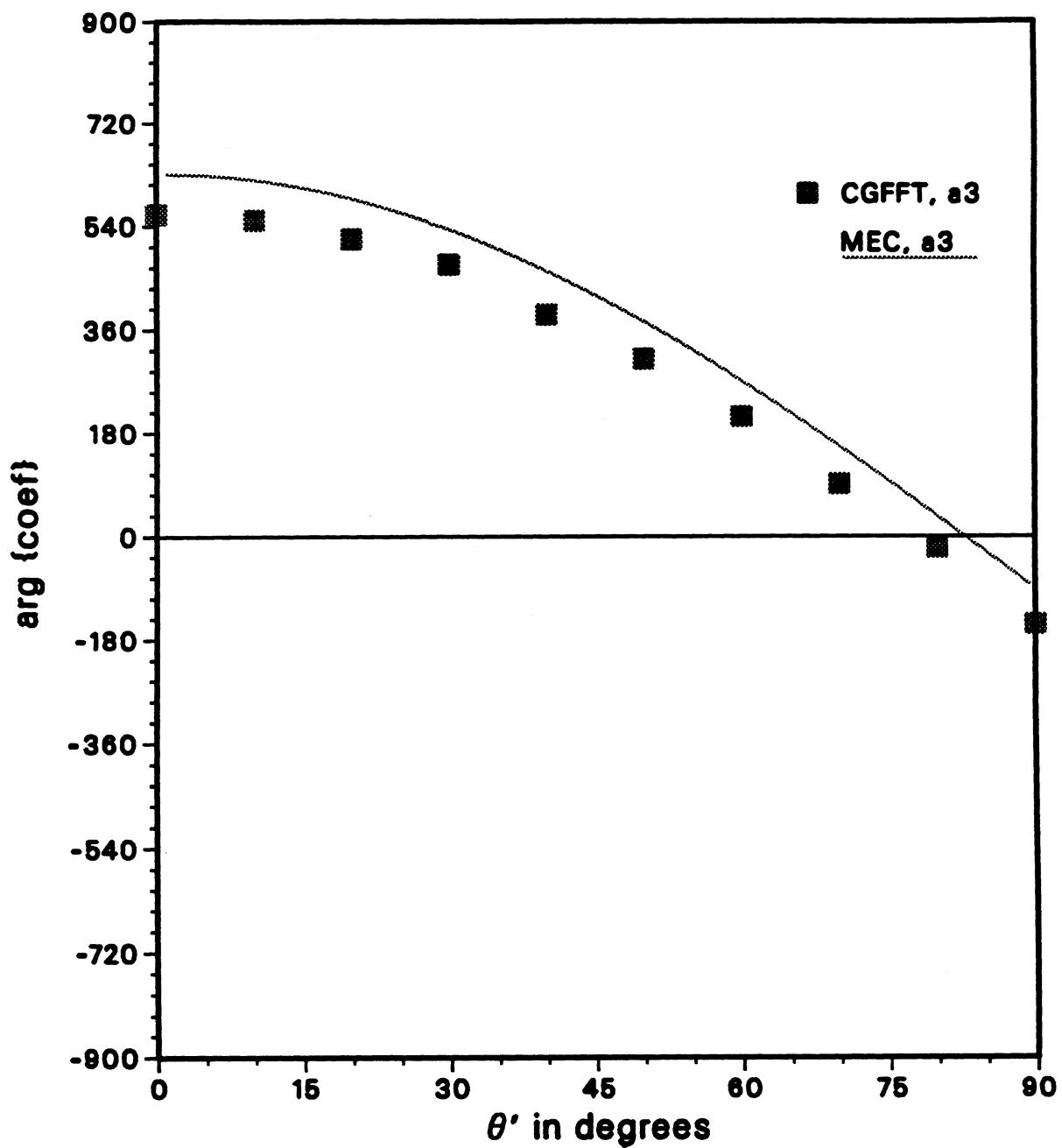
Figure 16.   E-polarization, coefficient c(θ')

for edge 2 of the plate, W=2λ, L=4λ.
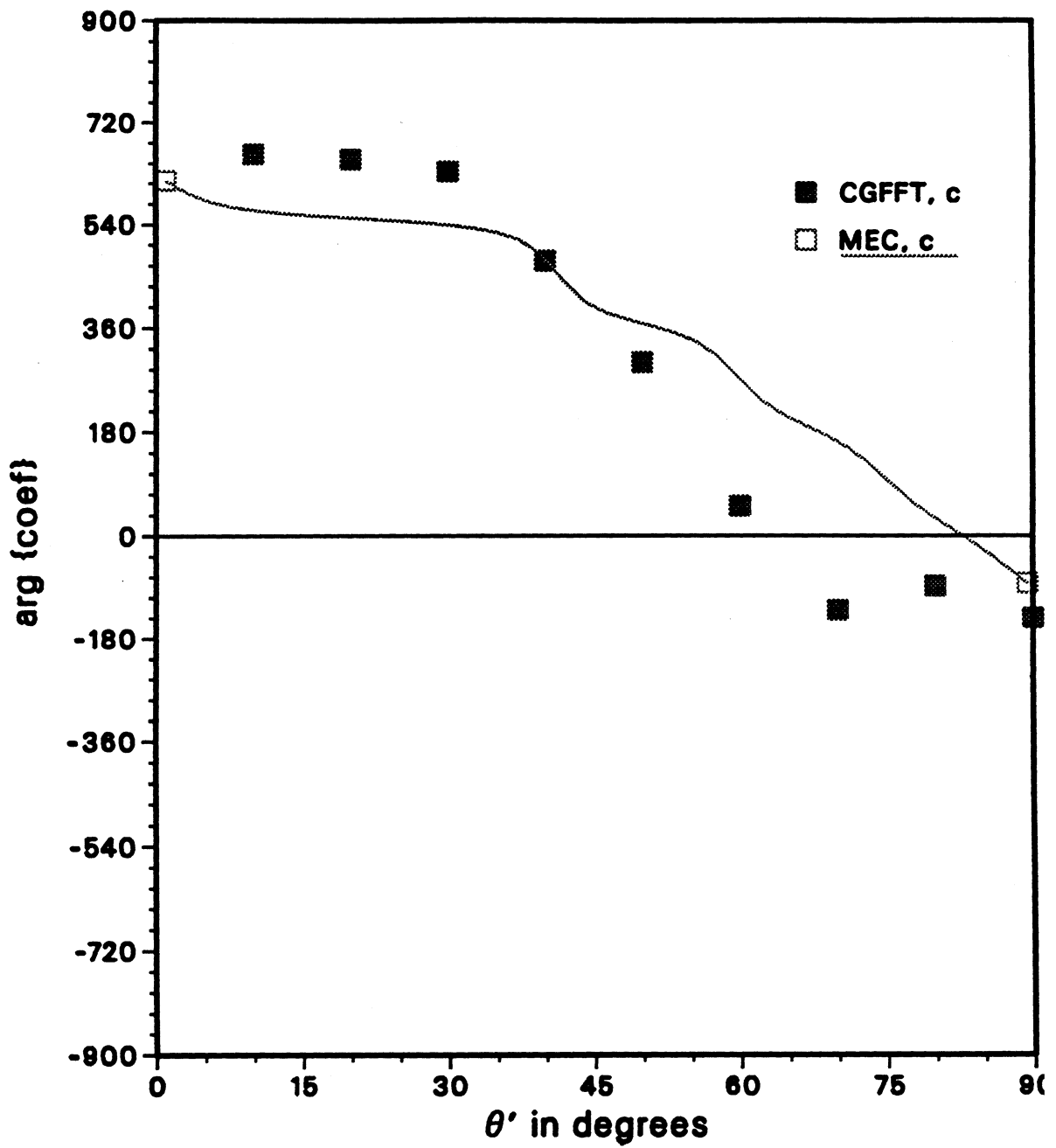
Figure 16b. E-polarization, coefficient c(θ')

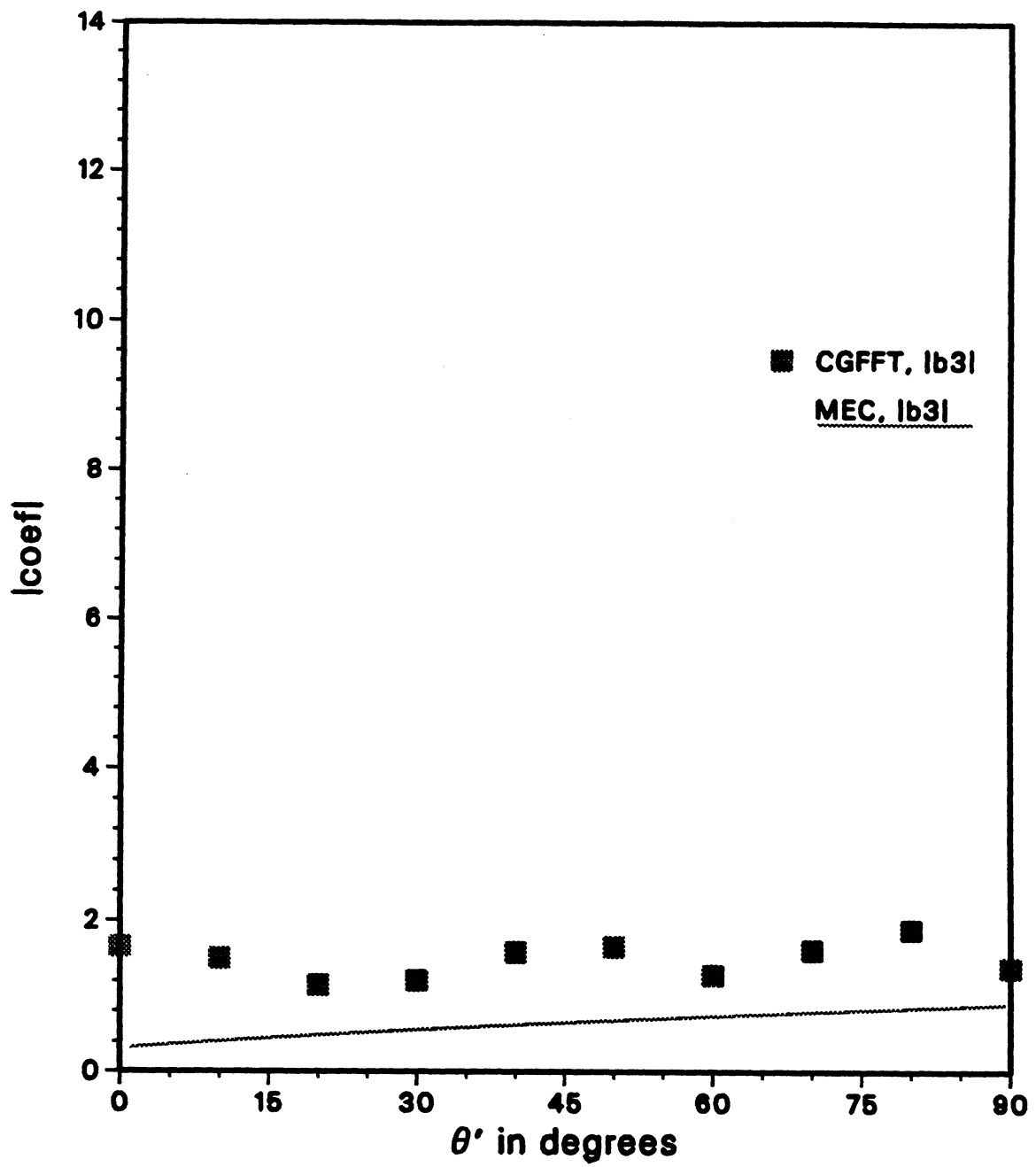for edge 2 of the plate, W=2λ, L=4λ.

Figure 17. H-polarization, side edge current on edge 2 of the plate, $\theta' = 10°$, W=2λ, L=4λ.

Figure 17b. H-polarization, side edge current on edge 2 of the plate, $\theta' = 10°$, W=2λ, L=4λ.

Figure 18. H-polarization, side edge current on edge 2
of the plate, $\theta' = 60°$, W=2λ, L=4λ.

Figure 18b. H-polarization, side edge current on edge 2
of the plate, $\theta' = 60°$, W=2λ, L=4λ.

Figure 19.   E-polarization, side edge current on edge 2
of the plate, $\theta' = 10°$, W=2λ, L=4λ.

Figure 19b. E-polarization, side edge current on edge 2
of the plate, $\theta' = 10°$, W=2λ, L=4λ.
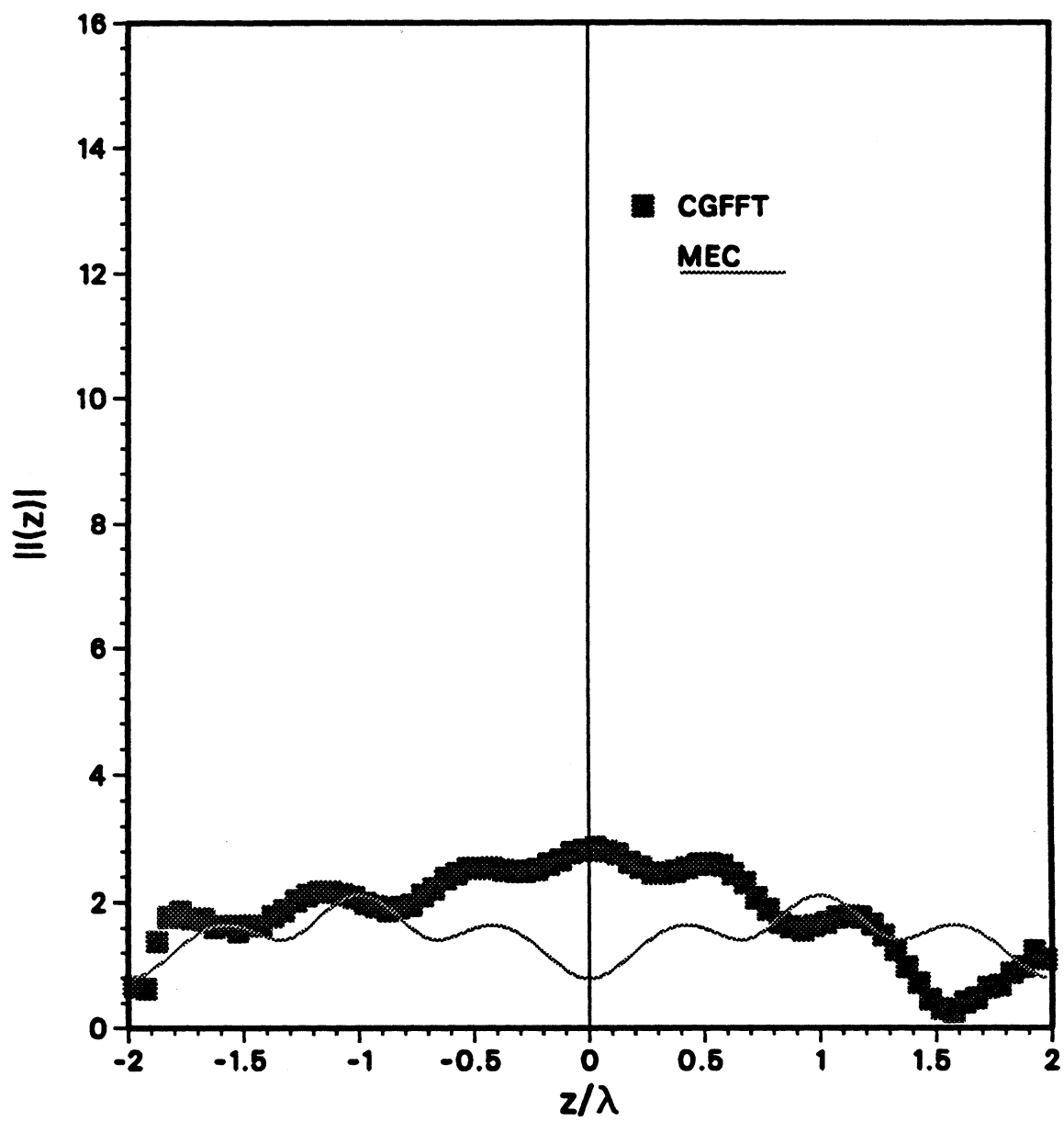
Figure 20. E-polarization, side edge current on edge 2
of the plate, $\theta' = 60°$, W=2λ, L=4λ.
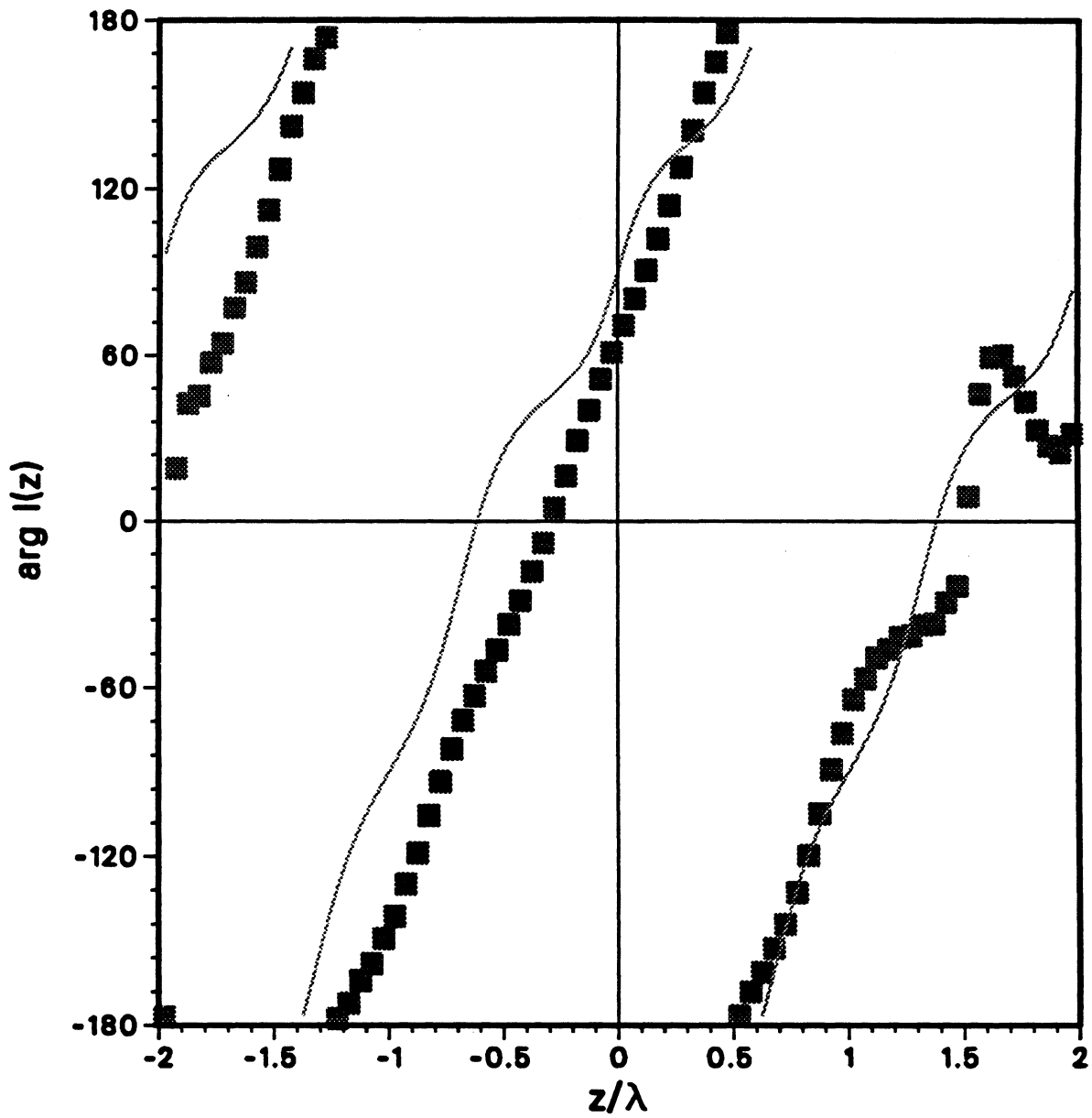
Figure 20b. E-polarization, side edge current on edge 2
of the plate, $\theta' = 60°$, $W = 2\lambda$, $L = 4\lambda$.

Figure 21.   E-polarization, coefficient a(θ')
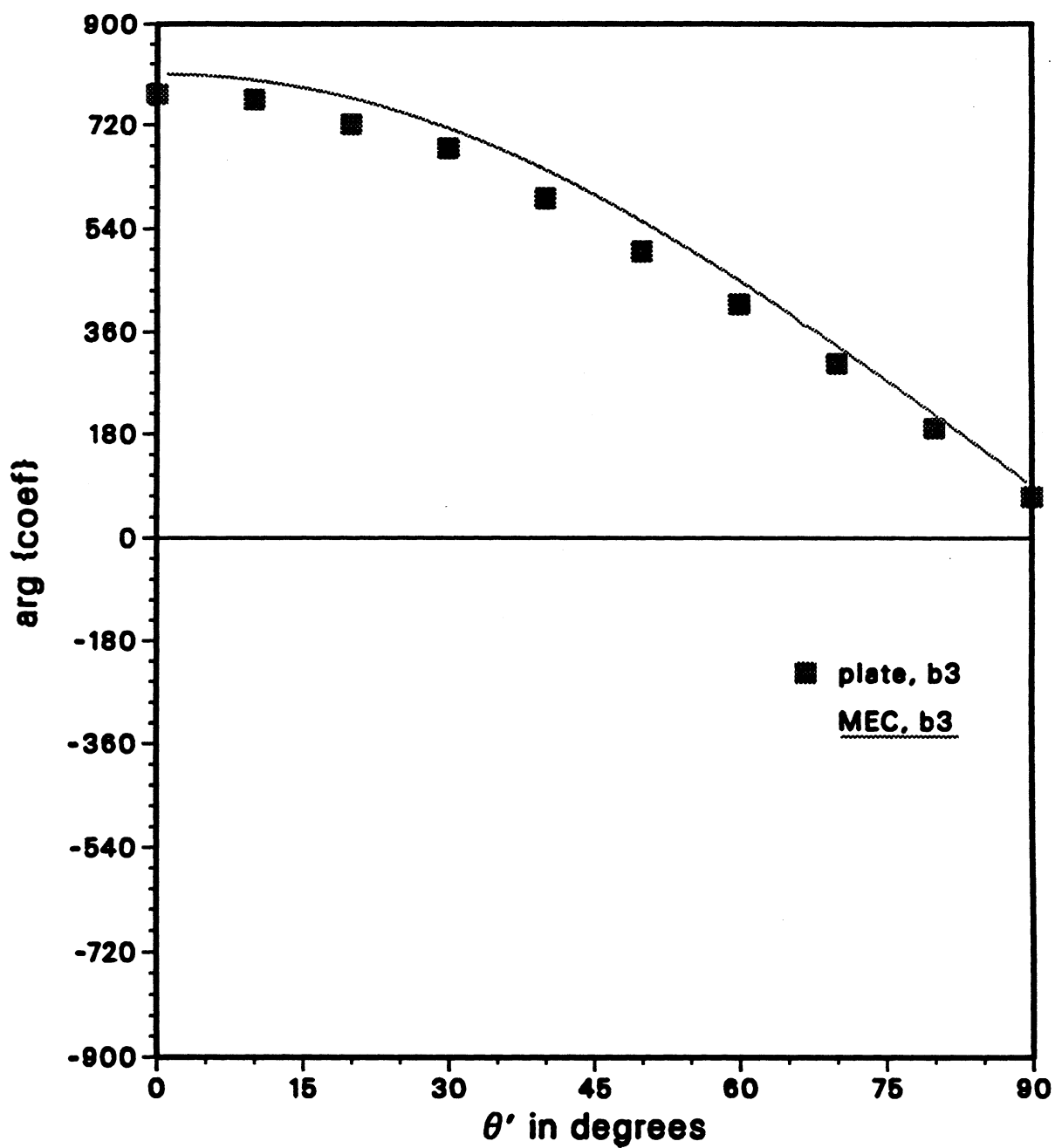
for edge 3 of the plate, W=2λ, L=4λ.

Figure 21b. E-polarization, coefficient a(θ')

for edge 3 of the plate, W=2λ, L=4λ.

Figure 22.   E-polarization, coefficient b(θ')
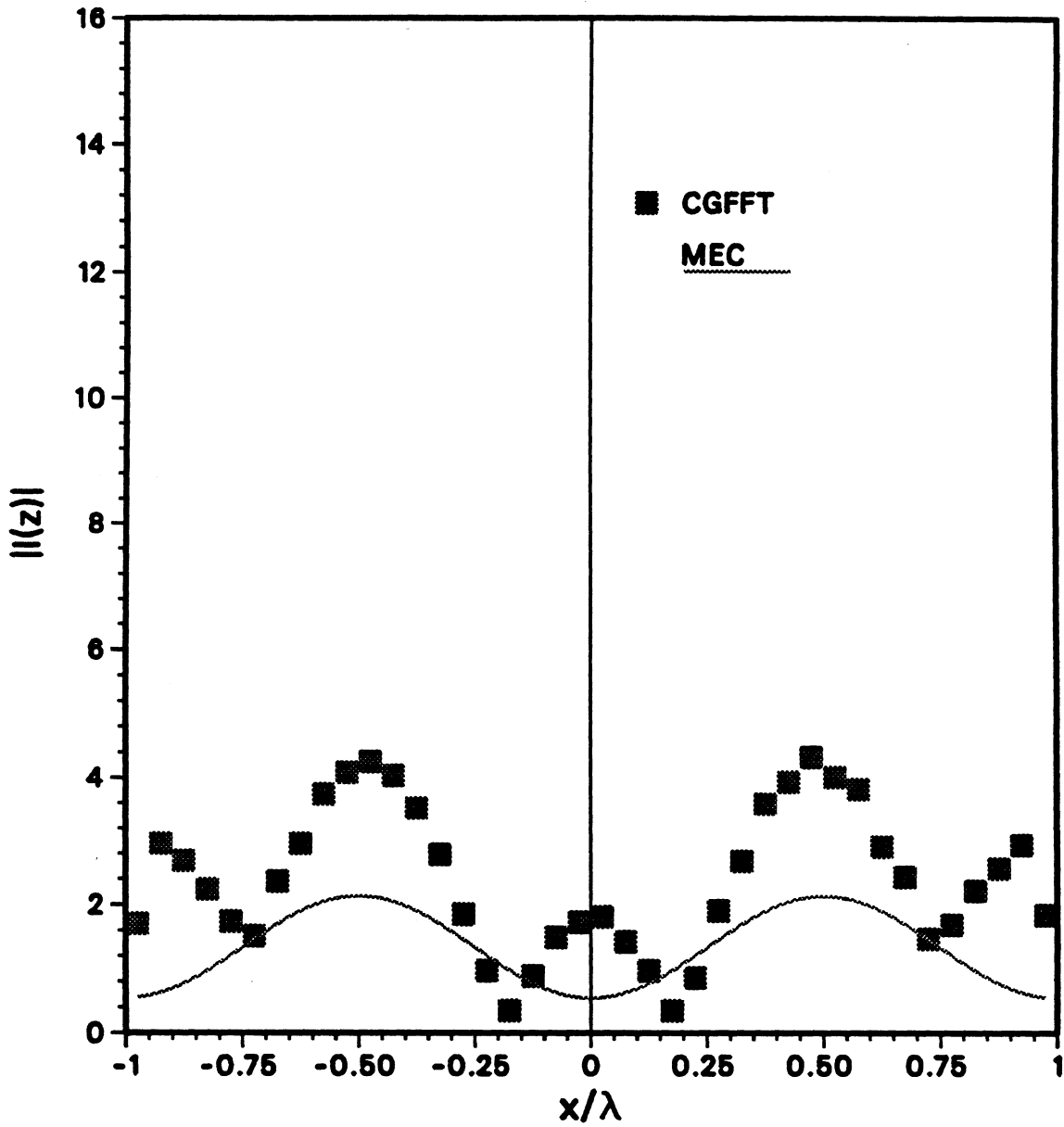
for edge 3 of the plate, W=2λ, L=4λ.

Figure 22b. E-polarization, coefficient b(θ')

for edge 3 of the plate, W=2λ, L=4λ.

Figure 23. E-polarization, current on edge 3
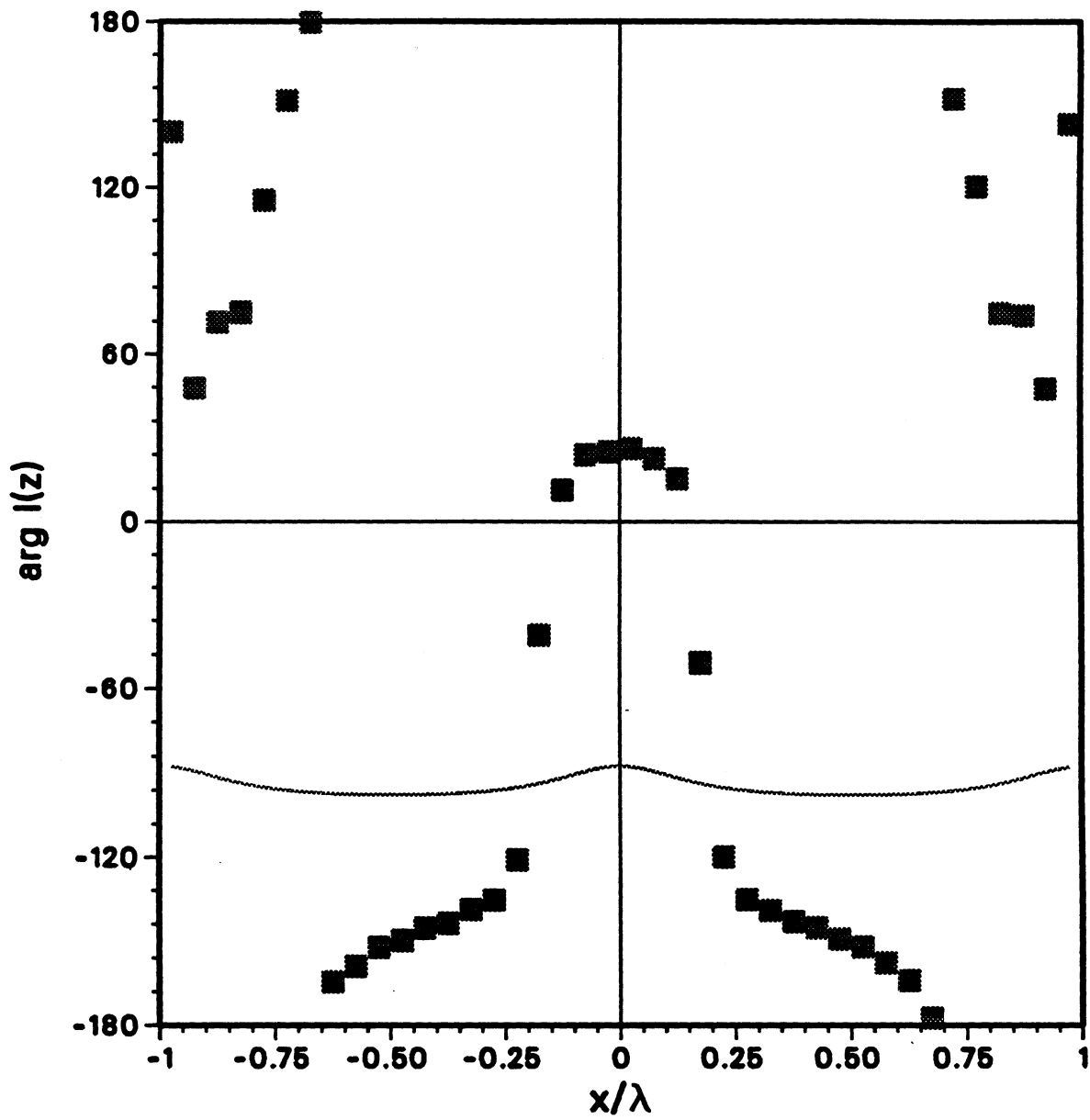
of the plate, $\theta' = 10°$, W$=2\lambda$, L$=4\lambda$.

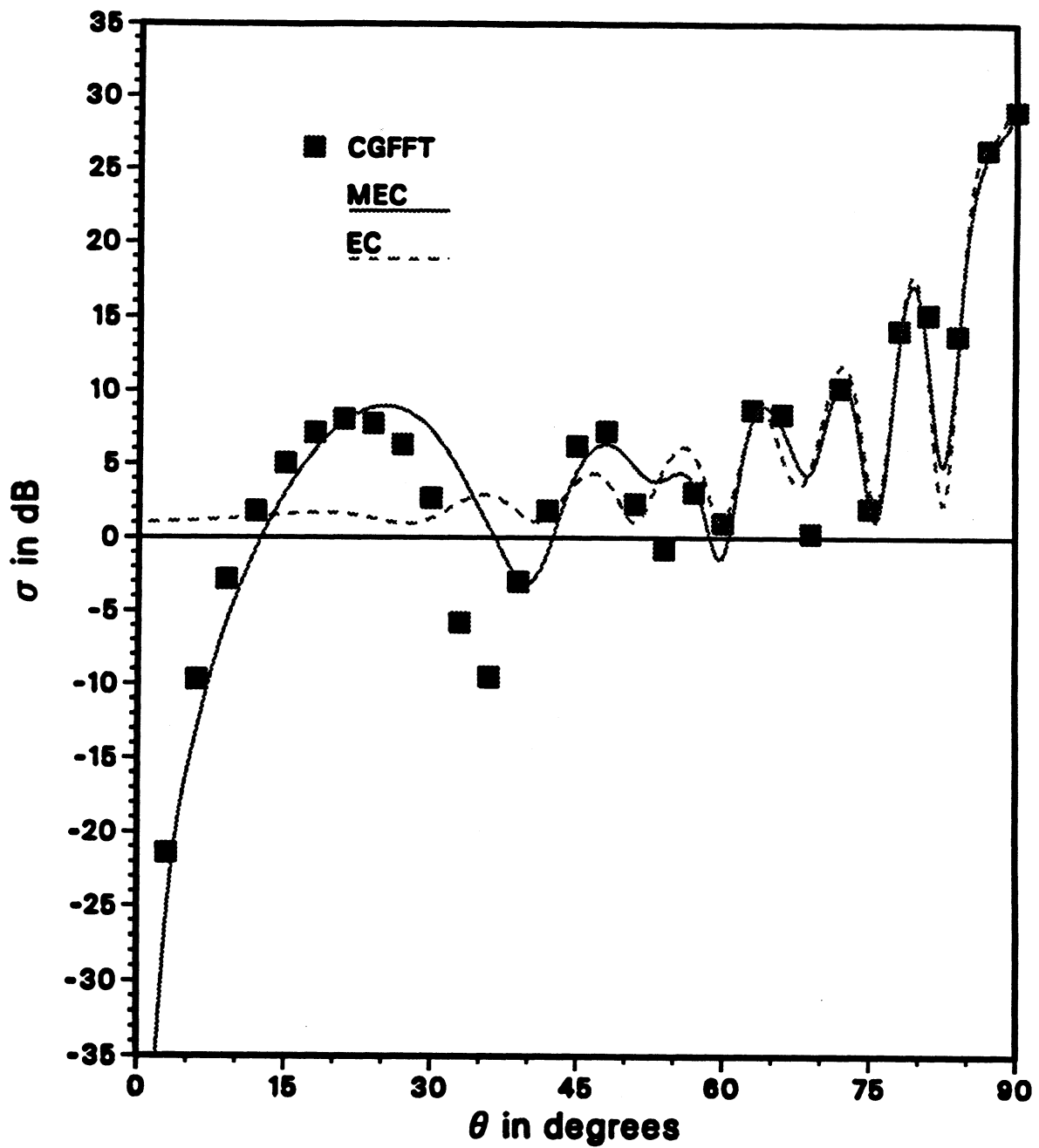Figure 23b. E-polarization, current on edge 3
of the plate, $\theta' = 10°$, W=2λ, L=4λ.

Figure 24. H-polarization, backscatter from a rectangular plate, L=4λ, W=2λ.
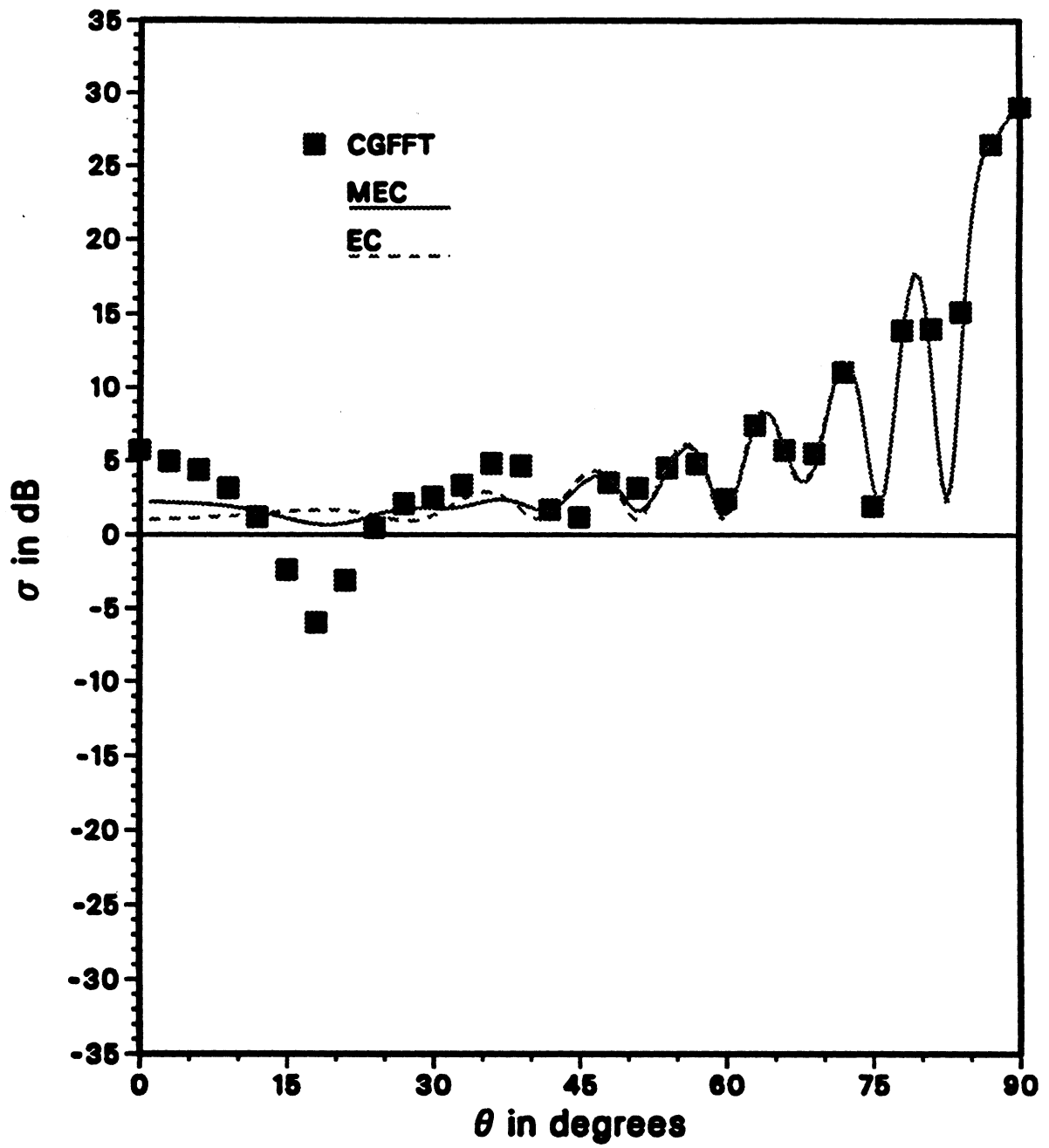
Figure 25. E-polarization, backscatter from a rectangular plate, L=4λ, W=2λ.